Heat transfer coefficient correlations of water subatmospheric vaporization in a channel of a smooth plate heat exchanger, based on Vaschy-Buckingham theorem

Pape Sène, Florine Giraud, Mamadou Lamine Sow, Brice Tréméac

Heat transfer coefficient correlations of water subatmospheric vaporization in a channel of a smooth plate heat exchanger, based on Vaschy-Buckingham theorem

Pape Sène [a], Florine Giraud [b,c], Mamadou Lamine Sow [a], Brice Tréméac [b, *]

[a] GREST (Groupe de Recherche sur l'Energie Solaire et les Transferts), LMFA (Laboratoire de Mécanique des Fluides et Applications), Département de Physique, Faculté des Sciences et Techniques, UCAD, Dakar Fann BP-5005 (Sénégal).

[b] Lafset (Laboratoire du froid et des systèmes énergétiques et thermiques), Cnam, HESAM Université, 292 rue Saint-Martin 75003 Paris (France).

[c] LOCIE, Université Savoie Mont Blanc, CNRS UMR5271, Savoie Technolac, 73376 Le Bourget Du Lac, France

[*]E-mail address: brice.tremeac@lecnam.net (Brice Tréméac)

Abstract:

Water as an environmentally friendly, safe and cheap natural refrigerant (R-718) requires vaporization conditions at sub-atmospheric pressures (~1 kPa). At these pressure ranges, studies on the specific vaporization of water are scarce and insufficient. For this reason, the engineering of heat exchangers using R-718 as working fluid remains empirical. The aim of this paper is thus to provide correlations to estimate water pool boiling and falling film evaporation heat transfer coefficient under subatmospheric pressure. Correlations developed are believed to be more widely used by providing dimensionless numbers consistent with phase-change phenomena occurring at sub and at-mospheric pressure. To develop these correlations, heat transfer phenomena during water vaporization at pressures ranging from 0.7 to 1.7 kPa in a scale-lab size (0.2 m wide x 0.5 m high) vertical smooth plate evaporator channel are studied. Filling ratio vary from 1/2 to 1/10 of the total channel height, canal thicknesses are set to 2 mm, 4 mm or 6 mm. Thus, raw experimental data from 139 tests performed under various operating conditions of a thermosyphon loop mimicking a sorption system are exploited. Each test consists of more than 1200 values. A graphical and statistical comparison between the heat transfer coefficient (HTC) obtained from the experimental database and the HTC estimated by empirical correlations from the literature is made, calculating the percentage of predicted data within an error band of ± 30% (τ_{30}), the mean absolute error (MAE), the mean relative error (MRE) and the correlation coefficient (r). Two methodical correlations for predicting the HTC of pool boiling and liquid film evaporation, are developed. They predict 86% (with MAE = 19%, MRE = 3%, $r = 0.79$) and 83% (with MAE = 18%, MRE = 2%, $r = 0.84$) of the experimental data in τ_{30} respectively. To extend their validity domains, the proposed correlations are evaluated using independent experimental data from the literature. Giving satisfactory results, it constitutes a first step towards the development of tools used for the sizing and the optimization of the design of two-phase heat exchangers.

Keywords: water vaporization, subatmospheric pressure, heat transfer coefficient, correlation, plate-type heat exchanger.

NOMENCLATURE

Latin letters

A	cross section $[m^2]$
c_p	thermal mass capacity $[J.kg^{-1}.K^{-1}]$
d_b	bubble diameter [m]
D_h	hydraulic diameter [m]
e	thickness [m]
g	gravity acceleration $[m.s^{-2}]$
G	mass velocity $[kg.m^{-2}.s^{-1}]$
h	heat transfer coefficient $[W.m^{-2}.K^{-1}]$
H_l	height of the liquid column [m]
L_c	capillary length $= \sqrt{\sigma/[(\rho_l - \rho_v)g]}$ [m]
P	pressure [Pa]
P_r	pressure ratio $[-]$
r	correlation coefficient $[-]$
$\dot{Q}$	heat flux [W]
$\dot{q}$	heat flux density $[W.m^{-2}]$
q_r	heat flux ratio
S	exchange area $[m^2]$
T	temperature [K]
MAE	Mean Absolute Error [%]
MRE	Mean Relative Error [%]

Greek Letters

Δh_{lv}	enthalpy of liquid-vapour change of state $[J.kg^{-1}]$
ΔT	temperature difference [K]
τ_{30}	percentage of predicted data within ±30% [%]
λ	thermal conductivity $[W.m^{-1}.K^{-1}]$
μ	dynamic viscosity $[N.m^{-2}.s]$
σ	surface tension $[N.m^{-1}]$
δ	characteristic length [m]
ρ	density $[kg.m^{-3}]$
φ	instrumental error (–)

subscripts

acq	relative to the acquisition system
b	boiling
cool	cooling
crit	critical
exp	experimental
f	film
fs	secondary fluid
in	inlet
instr	relative to the instrument
ir	intermittent region
l	liquid
out	outlet
p	plate
sat	saturation
pbr	pooling boiling region
pred	predicted

v	vapor
vr	vapor region
w	wall
z	zone

Dimensionless numbers

Bo	Bond Number $[-]$
Ca	Capillary number $[-]$
Co	confinement number $[-]$
F^*	Form factor $[-]$
μ^*	dynamic viscosities ratio $[-]$
Nu	Nusselt number $[-]$
Pr	Prandtl number $[-]$
ρ^*	density ratio $[-]$
ρ_v^*	vapor density ratio$[-]$
We	Weber number $[-]$

1. Introduction

In a context where regulations on synthetic refrigerants are becoming more and more restrictive due to their negative impact on the environment, it is urgent to think about the development of compact, efficient and "clean" refrigeration technologies. Thus, through the improvement of components such as the evaporator or the compressor, systems using natural refrigerants like water (R-718), represent a promising alternative. R-718 is an efficient fluid (high vaporization enthalpy and heat capacity), available, non-toxic, non-flammable, inexpensive, inert for the environment (ODP: Ozone Depletion Potential and GWP: Global Warning Potential are zero) and easy to handle (minimizes safety precautions) [1] [2]. Although the use of water as working fluid is widespread in sorption systems and is gaining ground in mechanical vapor compression systems equipped with turbo compressors [3], systems using water as refrigerant still shows poor performances partly due to the poor performance of the heat exchanger [4]. These poor performances could be mostly explained by the fact that using R-718 as refrigerant requires vaporization conditions at sub-atmospheric pressures (~1 kPa).

Indeed, the evaporator is the essential component of thermal machines since the maximum permissible heat exchange rate depends on its pressure conditions (thermophysical properties of the refrigerant) and on the topography of its heat exchange surfaces. However, at subatmospheric pressure ranges, the specificity of the thermophysical properties of R-718 and in particular its low vapour density ($\rho_v = 0.009\ \mathrm{kg.m^{-3}}$ and $\rho_l = 999.68\ \mathrm{kg.m^{-3}}$ at 1.2 kPa versus $\rho_v = 0.598\ \mathrm{kg.m^{-3}}$ and $\rho_l = 958.34\ \mathrm{kg.m^{-3}}$ at 101,325 kPa), lead to atypical boiling behaviours such as the appearance of bubbles of centimetric size often referenced in the literature [5] [6]. For example, at 1.2 kPa, the typical working pressure of chillers using R-718, mushroom-shaped bubbles of 15 cm in diameter can be observed under pool boiling conditions, in contrast to the spherical or semi-spherical bubbles of a few millimeters that can be observed at atmospheric pressure [4]. Due to this atypical behavior, correlations and design usually used to realize heat exchangers of thermal systems do not allow a proper sizing of R-718 evaporators. The needs to improve the efficiency of said machines using R-718, makes it essential to size correctly, optimize and reduce the size of heat exchangers, especially the evaporator.

In the evaporator, the refrigerant exchange heat from a source, through a process of vaporization (boiling or evaporation). This exchanger can be made of tubes and shells, fins or plates. Among the latter, smooth plate heat exchangers can be good candidates. The use of

vertical flat plate and falling film heat exchangers is especially attractive for sorption machines and potentially increases their compactness, reduces their weight and price compared to conventional vertical or horizontal tube configurations [4] [7]. The interest of these types of exchangers is also due to their unique advantages such as flexible thermal design (plates can be simply added or removed to meet different thermal services or process requirements), low manufacturing cost, ease of inspection and cleaning to maintain strict hygienic conditions, reduced load, better heat transfer performance due to fluid distribution over the plates, compactness, etc. [8] [9] [10]. Plate heat exchangers are also suitable for standardization of the manufacturing process [5]. Also, their deep channels, large ports and possible laser welding allow for vacuum vaporization [18]. This is consistent with the fact that the use R-718, with its high boiling temperature at atmospheric pressure ($T = 100\ °C, P = 101.325\ kPa$), requires to operate at sub-atmospheric pressures close to its triple point ($T = 0.01\ °C, P = 0.61\ kPa$) [4] [11] in the part containing the evaporator. But, at these low pressures ranges, in addition to the observation of centimeter size mushroom bubbles, since the pressure at the free surface (P_{sat}) is small, the pressure induced by the liquid column ($P_{static} = \rho_l g H_l$) can be of the same order of magnitude as the system pressure [5] [12]. Several experimental studies ([4] [13] [12] [14] [15]) confirmed the non-negligible influence of the liquid height (hydrostatic pressure) on the heat transfers during low-pressure pool boiling. The filling level (H_l) can therefore no longer be neglected in the analysis of heat transfer phenomena, as is commonly practiced for higher pressures. This is all the more important since the presence of this hydrostatic pressure causes the vapor bubbles to form in an inhomogeneous medium in pressure or subcooling [4]. Thus, the thermophysical properties of the refrigerant present strong variations [6], leading to phenomena of a certain complexity regarding thermal couplings and two-phase flows.

As a first approach towards the understanding of these complex phenomena and in order to design compact evaporators for sorption coolers and optimize their size, Giraud et al. [5] [16] [17] conducted experimental studies on the vaporization of water at subatmospheric pressure in a vertical smooth plate evaporator (VSPE) (scale-lab size: 0.2 m wide x 0.5 m high). Filling ratio (H_l) vary from 1/2 to 1/10 of the total channel height, the thicknesses (e) between two succeeding plates are set to 2 mm, 4 mm or 6 mm. The authors [5] mainly highlighted three different working zones: a boiling zone, a liquid film evaporation zone and a vapor zone. Their results are in perfect agreement with the observations of Chang et al. [13]. The liquid film evaporation zone is due to the free surface moving due to boiling as well as the spread of the encapsulated liquid contain between the bubbles and the free surface. This liquid is spread over the top wall plate and forms the liquid film that evaporates immediately [5] [13]. The liquid film evaporation zone is the seat of more than 70% of the heat transfer in the VSPE [17]. Studying the effect of the channel thicknesses on the VSPE performance, the authors also observed, for a confinement number $Co = \frac{1}{D_h} \cdot \sqrt{\frac{\sigma}{g(\rho_l - \rho_v)}} = 0.69\ (e = 2\ mm)$, phenomena such as droplet entrainment by the steam flow [16] . They confirmed experimentally the impact of this observation on the heat transfer: higher performances are observed for a confinement number $Co = 0.69$ compared to a confinement number $Co = 0.35\ (e = 4\ mm)$ and $Co = 0.23\ (e = 6\ mm)$ when droplets entrainment is observed, i.e. for high rate of steam production obtained at high entrainment pressures and low filling rate. Then, as a first tool toward the design of compact subatmospheric VSPE, Giraud et al [17] developed dimensionless numbers depending on the measured cooling capacity, the thermophysical properties of the fluid and the operating conditions. They showed that, using these dimensionless number, similar evaporator behavior could be observed for different boiling phenomena kinetics since they show that, based on these numbers, the evaporator behavior is similar when the evaporator is included in a thermosyphon loop than when it is included in an ad-sorption system.

Despite the efforts made, efforts still should be made to develop more universal correlations involving in particular a form factor and exchange coefficients. However, the knowledge on the vaporization of water at subatmospheric pressure remains scarce and insufficient and, given the great difference between the characteristics of subatmospheric vaporization and those observed at atmospheric pressure [4] [6], the dimensionless numbers usually used at high pressure are not sufficient to properly predict phenomena observed at subatmospheric pressure. Empirical correlations of the literature developed, verified or adapted to low pressure conditions, are then limited mainly because they do not consider all the independent physical quantities that govern the confined vaporization at subatmospheric pressure such as the form factor (hydrostatic pressure), the inhomogeneous pressure condition of the medium (variation of the thermophysical properties of the refrigerant), the boundary conditions, etc. Moreover, the dimensional analysis adopted for the elaboration of the said correlations, in general, does not verify the independence of the physical quantities despite the necessity to ensure that no physical quantity, apart from the variable of interest, depends on the variation of the other quantities [18]. This independence is a key factor for dimensional analysis modeling since it allows an easily transferred results from one scale to another (similarity).

Referring to the observations of literature, the understanding of heat transfer phenomena during pool boiling and liquid film evaporation at sub-atmospheric pressure thus seems fundamental for optimizing design and performances of compact heat plates exchangers. For this purpose, heat exchanger designers inevitably have a great need for methodical HTC correlations based on rigorous dimensional analysis and offering higher accuracy than existing correlation. This is what the paper attend to do: offering correlations with dimensionless numbers requires for the proper design of subatmospheric water heat exchanger. It is believed, that although the obtention of the coefficient may remain empirical, the used of the chosen dimensionless numbers lead to universal correlations since it includes the independent physical properties influencing phase change phenomena at low and high pressure.

The approach starts with a presentation of the HTC correlations available in the open literature. Subsequently, the raw experimental database and the experimental set up used by Giraud et al. [16] to determine the heat transfer coefficients during pool boiling and liquid film evaporation of water at sub-atmospheric pressures is described. The constant and the exponents of the general or Dittus-Boelter type and other relevant correlations from the literature [19] is fitted to the database obtained from the experimental results of Giraud et al. [16] for graphical and statistical comparison between the experimental HTC and the HTC estimated. Then, based on the scientific knowledge generated by previous studies, new methodical correlations for predicting HTC during pool boiling and evaporation of the liquid film falling from water in a VSPE is developed. These correlations are based on a rigorous dimensional analysis approach, following Vaschy-Buckingham theorem described by Delaplace et al. [18]. The news proposed correlations consider, among others, the form factor (canal thickness and filling ratio), the thermophysical properties of refrigerant (hydrostatic pressure and saturation pressure), the heat flux density and the parietal superheating. The obtained results are presented and discussed. Then, in order to extend the range of validity and test the robustness of the developed correlations, these models are fitted and evaluated using independent experimental data from the literature.

2. HTC correlations of literature

In this section, different relevant correlations commonly used to predict HTC during water vaporization are presented and discussed. There are many correlations in the literature for

estimating the HTC during water vaporization, but many of them are valid only for typical heat transfer surface topography and/or operating conditions (high pressure). The main parameters affecting nucleate boiling are heat flux, saturation pressure, thermophysical properties of the working fluid and characteristics of the boiling surface and material etc. [20]. Thus, Dittus-Boelter [19], Labuntsov [11], Kruzylin [11], Stephan-Abdelsalam [11], Chang (pool boiling region and intermittent region) [13], Mc Nelly [21] and Yu [20] correlations consist of parameters that influence water vaporization.

The general or Dittus-Boelter type correlation (Eq. 1) [19] which relates the Nusselt number (Nu) to the Reynolds (Re) and Prandtl (Pr) numbers, is frequently used to estimate the HTC in heat exchangers. Several authors use this ready-made correlation and adjust the coefficients (C) and exponents (a, b) to be close to their experimental results.

$$\frac{h\,\delta}{\lambda_l} = C \cdot \left(\frac{\rho_l\, U\, \delta}{\mu_l}\right)^a \cdot \left(\frac{\mu_l\, c_p}{\lambda_l}\right)^b \tag{1}$$

As a first approach toward a generalization of correlations, efforts are made by [13] [11] [21] and [20] in developing empirical models of HTC or testing existing correlations in pool boiling at low pressure conditions. However, from these studies, only those in [13] could be apply to heat exchange in the context of a plate evaporator.

Zajaczkowski et al. [11] conducted experimental studies on the influence of subatmospheric pressure and heat flux density on water nucleate boiling. Experiments were conducted above a copper plate in an insulated glass cylinder. Pressure ranges between 1 to 10 kPa, and heat fluxes between 10 and 45 kW/m^2. As a main result, they showed that accurate approximations of the experimental heat transfer coefficient are obtained using the Labuntsov correlation (Eq. 2) (Mean Absolute Deviation (MAD 0.12-0.89), the Kruzylin correlation (Eq.3) (MAD 0.25-0.35) and the Stephan-Abdelsalam correlation (Eq. 4) (MAD 0.16). Thus, Labuntsov correlation (Eq. 2) and Kruzylin correlation (Eq. 3) directly determines the heat transfer coefficient as a function of some thermophysical properties of the fluid, the saturation temperature and the heat flux. Stephan-Abdelsalam correlates (Eq. 4) the Nusselt number as a function of dimensionless numbers that take into account the heat flux and several thermophysical properties of the fluid.

$$h = 0.075 \cdot \dot{q}^{0.67} \cdot \left(1 + 10 \cdot \left(\frac{\rho_v}{\rho_l - \rho_v}\right)^{0.67}\right) \cdot \left(\frac{k_l^2}{\nu \cdot \sigma \cdot T_{sat}}\right)^{0.33} \tag{2}$$

$$h = 0.0777 \cdot \left(\frac{\rho_v\, \Delta h_{lv}}{\rho_l - \rho_v}\right)^{0.33} \cdot \left(\frac{\rho_l}{\sigma}\right)^{0.33} \cdot \left(\frac{k_l^{0.75} \cdot \dot{q}^{0.7}}{\mu_l^{0.45} \cdot c_{p,l}^{0.12} \cdot T_{sat}^{0.37}}\right) \tag{3}$$

$$h = 0.23 \cdot \frac{k_l}{d_b} \cdot \left(\frac{\dot{q}\, d_b}{k_l\, T_{sat}}\right)^{0.674} \cdot \left(\frac{\rho_v}{\rho_l}\right)^{0.297} \cdot \left(\frac{\Delta h_{lv}\, d_b^2}{\left(\frac{k_l}{\rho_l\, c_{p,l}}\right)^2}\right)^{0.371} \cdot \left(\frac{\left(\frac{k_l}{\rho_l\, c_{p,l}}\right)^2 \rho_l}{\sigma\, d_b}\right)^{0.35} \cdot \left(\frac{\rho_l - \rho_v}{\rho_l}\right)^{-1.73} \tag{4}$$

Stephan-Abdelsalam correlation (Eq. 4) is one of the most used correlations in the literature. However, in this equation, bubble diameter (d_b) is sometimes very difficult to predict. The authors recommend using the Fritz correlation (Eq. 5) for prediction of the bubble diameter as the following [22].

$$d_b = 0.0146 \cdot \theta \cdot \left(\frac{2\,\sigma}{g(\rho_l - \rho_v)}\right)^{0.5} \quad (5)$$

In which the contact angle θ is specified equal to 45° for water and 35° for other liquids studied by the author [22]. In their calculations, Zajaczkowski et al. [11] set a contact angle θ equal to 35°.

Chang et al. [13] studied the thermal performance and behavior of an evaporator consisting of a pair of parallel stainless steel plates of 138 x 20.8 mm² each with 10 mm channels. The evaporator is inserted in a two-phase thermosiphon loop. The pressure varied between 2.1 kPa and 66.2 kPa. In their experiments, the authors observed three distinct flow regions with different heat transfer properties. They developed a set of three HTC correlations for each region : pool boiling region (Eq. 6), intermittent region (Eq. 7) and vapour region Eq. (8). Correlations for the pool boiling region (Eq. 6) and the intermittent region (Eq. 7) will be used. They allow the HTC of pool boiling and liquid film evaporation to be calculated from the heat flux and reduced pressure.

$$h_{pbr} = (1.951 \cdot 10^6 \cdot \dot{q}^{-0.26}) \left(\frac{P_{sat}}{P_{crit}}\right)^{(0.508 - 5.91 \cdot 10^{-6} \cdot q)} \quad (6)$$

$$h_{ir} = (2 \cdot 10^6 \cdot \dot{q}^{-0.325}) \cdot \left(\frac{P_{sat}}{P_{crit}}\right)^{(0.449 - 4.72 \cdot 10^{-6} \cdot q)} \quad (7)$$

$$h_{vr} = (2.06 \cdot 10^6 \cdot \dot{q}^{-0.412}) \cdot \left(\frac{P_{sat}}{P_{crit}}\right)^{(0.441 - 7.08 \cdot 10^{-6} \cdot q)} \quad (8)$$

Baki [21] performed a review on experimental boiling data at subatmospheric pressures for three different fluids, among them water, to compare them to four known correlations. His results showed poor accuracy between experimental and predicted data for three of the correlations. Only Mc Nelly correlation (Eq. 9) that determines the HTC from the heat flux, some thermophysical parameters of the fluid and the working pressure, gives satisfactory results (mean error of 40% and correlation coefficient (r) of 0.91).

.

$$h = 0.225 \cdot \left(\frac{q\, c_p}{\Delta h_{lv}}\right)^{0.69} \cdot \left(\frac{P\, \lambda}{\sigma}\right)^{0.31} \cdot \left(\frac{\rho_l}{\rho_v} - 1\right)^{0.32} \quad (9)$$

Yu et al. [20] experimentally estimated water boiling heat transfer coefficient obtained on a horizontal copper bar surface for a pressure range of 1.8-3.3 kPa and a heat flux range of $4000 - 10000\ W \cdot m^{-2}$. Based on their experimental data, the authors obtained, by regression, the following correlation (Eq.10). The correlation developed is a pressure and heat flux corrected version of the convective boiling correlation [14].

$$h = 0.226 \cdot P_r^{1.497} \cdot q_r^{1.023} \cdot \left(\frac{g\, \beta\, \Delta T\, L_c^3}{\mu_l^2}\right)^{-0.891} \cdot \left(\frac{\mu_l\, c_{p_l}}{\lambda_l}\right)^{0.578} \quad (10)$$

3. Test bench

Giraud et al. [16] performed an experimental study on a prototype refrigeration system developed at Lafset to simulate the operating conditions that could occur in machines using water as refrigerant (Fig.1). The test bench is a closed-loop thermosiphon, assisted by a pump. It consists mainly of two heat exchangers: an oversized condenser and a smooth plate evaporator. To form the classic circuit of a refrigerating machine, a liquid supply line and a steam exhaust line connect these two main components. Type K thermocouples (named T + a number), pressure sensors (named P + a number) and flowmeters (F1 and F2) are installed in the refrigerant circuit and in the two auxiliary circuits. The saturation temperatures inside the evaporator and the condenser are regulated by means of two heating/cooling devices (B1 and B2). A third heating device (B3) is used to adjust the fluid temperature at the inlet of the expansion valve to match the temperature of the refrigerant at the outlet of the condenser in a chiller. The condenser is a cylindrical steel vessel (304L stainless steel) with an inside diameter of 300 mm and a height of 720 mm insulated with the outside. An oversized copper tube coil heat exchanger is placed inside the container to condense the steam along the outer surface of the tube and store the refrigerant in liquid state. The condenser is used here to set driving pressures and simulate an absorber or compressor that would exist in a real chiller.

The entire test bench is made up with ISO-K component to allow high gas tightness. To limit the introduction of incondensable gas, before filling the condenser with water, the entire experimental setup is vacuumed during at least 12 hours and the condenser is then filled with an amount of water that was previously boiled. The condenser and then the entire experimental setup are regularly expunged of a part of the vapor phase, until the pressure measured is equal to the water saturation pressure at the measured temperature during at least one week.

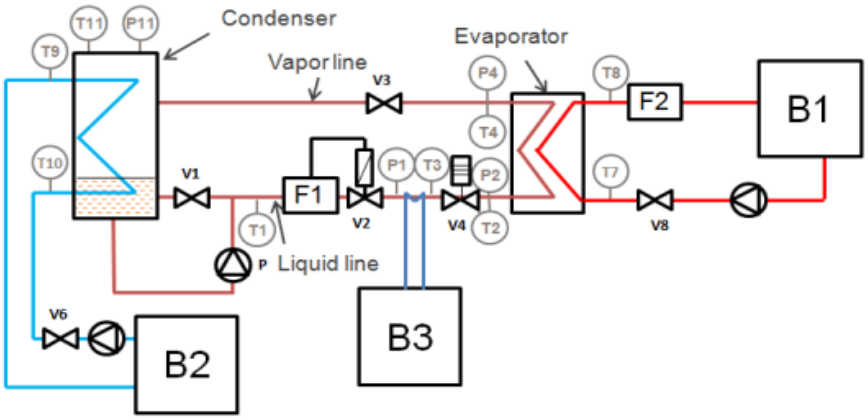

Figure 1 : Drawing of the pump-assisted thermosiphon loop used [16].

3.1. Evaporator

The present study focuses on the vaporization phenomena occurring in the evaporator (Fig.2a) of the test bench (Fig.1). This heat exchanger consists of three smooth plates 500 mm high and 200 mm wide. Two of these plates are made of steel (304L stainless steel), the third plate is made of polymethyl methacrylate (PMMA). The plates are placed in parallel so that they constitute vertical channels in which a primary fluid or refrigerant and a secondary fluid (hot source) circulate. These fluids, circulate in co-current from bottom to top. The central plate, separating the two channels, ensures heat exchange between the two fluids. The channel formed between the two steel plates in which the secondary fluid flows is fixed at 1 mm. The thickness of the refrigerant circulation channel between the outer PMMA plate and the central plate can be set at 2, 4 or 6 mm according to the needs of the experiment, using an O-ring and the spacer. The refrigerant is fed through three capillary tubes with an inner diameter of 2 mm each, located at the bottom of the plate. This creates a water column, the height of which is deliberately set according to the needs of the experiment by means of monitoring.

The central plate is 6 mm thick and is the seat of 44 K type thermocouples (22 pairs facing each other - Fig.2b). A detailed configuration of a pair of thermocouples is shown in Fig. **3**. The thermocouples in each pair are recessed at intervals $l_1 = 4$ mm to measure the temperature distribution in the evaporator center plate (Fig.2a). The depths of the slots are identical and equal to $l_2 = 1$ mm (distance between the wall and the thermocouple $T_{1,i}$ and $T_{2,i}$). In this figure, $T_{1,i}$ represents the temperature measured by the thermocouple (i) on the refrigerant (primary fluid) side and $T_{2,i}$ the temperature measured by a thermocouple (i) on the secondary fluid side.

Due to the driving pressure imposed in the evaporator by the condenser (pressure set by the thermostatic bath B2) and the evaporator (pressure set by the thermostatic bath B1), vaporization (boiling) of the refrigerant occurs. The PMMA plate on the refrigerant side being transparent, the visualization of boiling phenomena occurring in the channel concerned is allowed and recorded by a high-speed camera (Phantom VEO410). Acquisitions are performed at 3000 images per second with a resolution of 1280 x 800 and an exposure time of 191.8 µs.

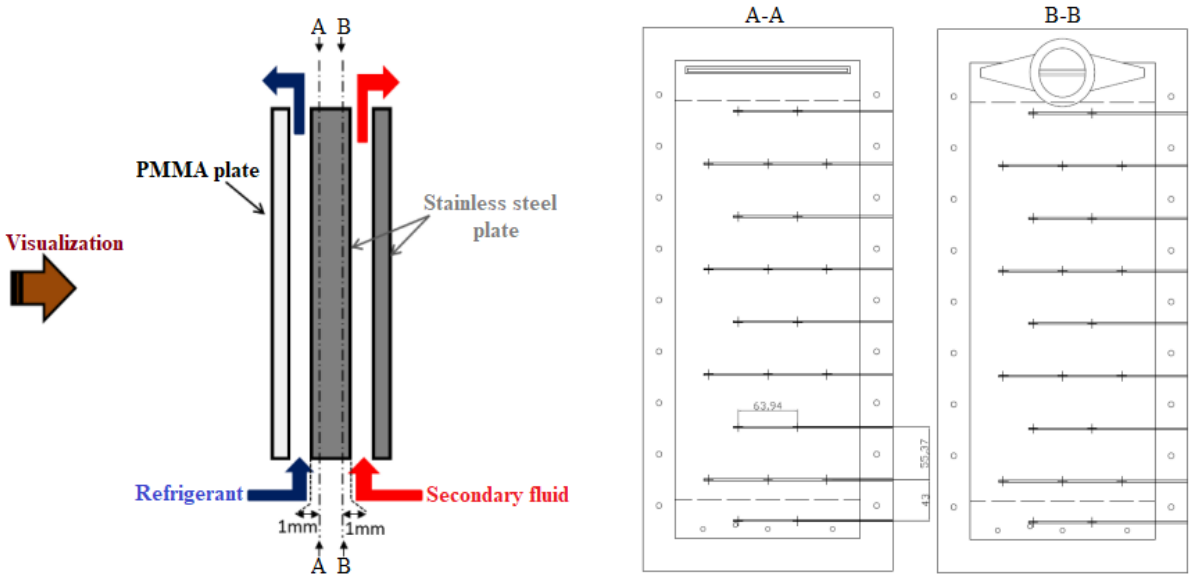

(a) (b)

Figure 2 : (a) Vertical smooth plate evaporator (VSPE); (b) Location of thermocouples located in the center plate.

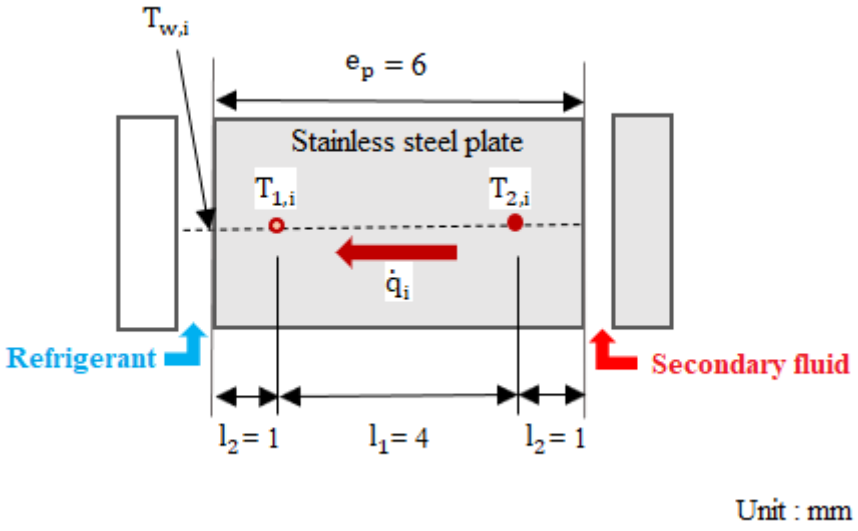

Figure 3: Configuration of a pair of thermocouples

Further information about the experimental procedure is presented by [16].

3.2. Experimental Uncertainties

A summary of the uncertainties is reported in Table 1. All instruments are connected to an acquisition system. The maximum error of the acquisition system is 0.02%. The uncertainties of the data are estimated by assuming that the instrumental error was uniformly distributed and could be estimated by Eq.11 as in [23] cited by [16].

$$u(a) = \frac{\varphi_{instr} - \varphi_{acq}}{\sqrt{3}} \quad (11)$$

Table 1 : Specification of the different measuring devices and standard data uncertainties associated.

Devices	Type	Accuracy of the device	Range	Data uncertainties
Thermometer	T-type thermocouple	0.1 K	- 10 to 85 °C	0.06 K
Refrigerant flow meter	Thermal mass flow meter	± 1% of full scale	0.04 - 2 kg h^{-1}	0.01 kg h^{-1}
Coolant flow meter	Electromagnetic flow meter	± 0.5% of reading	0.017 - 0.034 kg s^{-1}	0.00006 kg s^{-1}
Pressure measurement	Pressure transmitter with ceramic sensor	± 0.075% of reading	0 - 5 kPa	0.0009 kPa

3.3. Experimental program and data reduction

In order to estimate the impact of the thermophysical properties of the fluid, the heat flow, the parietal superheating, the filling height of the channel and the geometrical parameters on the HTC during the confined vaporization of water at subatmospheric pressure in a smooth plate heat exchanger, the raw experimental data obtained on the test bench (Fig.1) by Giraud et al. [16] is exploited. These data are determined as a function of the thickness e of the refrigerant vaporization channel. The database consists of 43 points for e = 2 mm, 48 points for e = 4 mm and 48 points for e = 6 mm. A total of 139 tests with 1200 values collected for each of them during at least 20 minutes once steady-state is obtained are exploited. Data obtained are then used to develop dimensionless number since they allow to vary internal measurements representing the causes (dimensionless number) and measuring their consequences on the heat transfer phenomena occurring in the smooth plate evaporator (Fig.2).

The experimental conditions covered are summarized in table 2.

Table 2 : Domain covered by the experimental test

Parameters	Field
Filling ratio	$[10-50]$ % (equivalent in $[5-25]$ cm)
Temperature set point at the condenser (bath B_2 - T_{fs})	$[2-15]$ °C (equivalent in an operating pressure of $[0.7-1.7]$ kPa)
Temperature set point at the thermostatic bath B3	$[30-45]$ °C (equivalent in a mass vapor quality inlet of $[1.7-3.8]$ %)
Temperature set point at the evaporator (bath B_1 - $T_{in,fs}$)	$[10-25]$ °C (equivalent in a driving pressure of $[0.3-2.1]$ kPa)
Channel thick (refrigerant side - e)	2 mm, 4 mm, 6 mm

Pressures, temperatures, flow rates etc. are recorded by a LabVIEW program, once the desired experimental conditions are ensured and steady-stated conditions are reached. Experimental data relevant to this study are:

- inlet temperature of the secondary fluid $T_{in,fs}$
- cooling capacity $\dot{Q}_{cool}$ which is calculated by a balance at the secondary fluid level,
- saturation pressures detected at the inlet and outlet of the evaporator refrigerant ($P_{in,\ ref}$ and $P_{out,\ ref}$),
- temperatures measured by the thermocouples on the secondary fluid side T_2 and on the refrigerant side T_1 etc.

Based on this data, a local heat flux is estimated assuming one directional heat flux and quasi-steady state conditions. This local heat flux is the heat flux estimated at the area where a pair of thermocouples is located. It is determined by the derivative of the one-dimensional heat conduction (Eq. 12).

$$\dot{q}_i = \lambda_p \frac{T_{2,i} - T_{1,i}}{l_1} \tag{12}$$

The average heat flow from the secondary fluid to the refrigerant for each zone (boiling zone, liquid film evaporation zone and vapor zone) is then determined by the Eq. 13.

$$\dot{q}_z = \frac{S}{l_p\ H_z} \sum_{i=1}^{n} \left(\lambda_p \frac{T_{2,i} - T_{1,i}}{l_1} \right) \tag{13}$$

Where $S = l_p * 0.05537 m^2$ is the area of the mesh around a thermocouple (elementary area), $l_p = 0.2$ m is the width of the plate, n is the maximum number of thermocouples in the considered zone, $\lambda_p = 16.3\ W.m^{-1}.K^{-1}$ is the thermal conductivity of stainless steel, assumed to be constant in the temperature range studied and H_z is the height of the considered zone. This considered zone is based on the previous observation of Giraud et al. [5], those identify four different working zones: a zone at the entrance of the channel where the thermal equilibrium is reached between the refrigerant and the secondary fluid and in which the incoming bubbles collapse, a boiling zone, a liquid film evaporation zone and a vapour zone (Fig. 4). Thus, heat flows are averaged by zone (i.e. a mean heat flow is estimated for the boiling area, one for the falling film are and one for the vapor area).

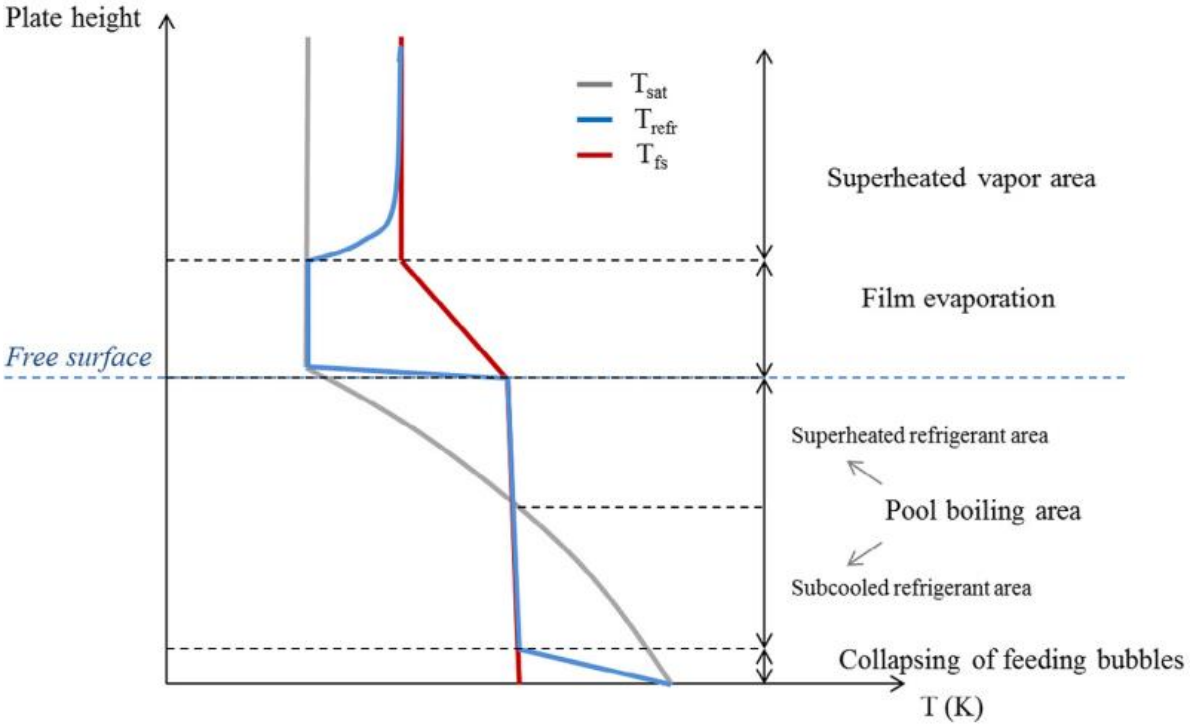

Figure 4: Schematic diagram of the temperature development of the secondary fluid and refrigerant as a function of evaporator height *[17]*

The local temperature at the plate wall $T_{w,i}$ in front of a thermocouple (i) on the refrigerant side (Fig. **3**) is calculated by extrapolation by Eq. (14).

$$T_{w,i} = T_{1,i} - \frac{\dot{q}_i \cdot l_2}{\lambda_p} \tag{14}$$

Thus, the average wall temperature for the considered area on the refrigerant side $T_{w,z}$ is then calculated by the Eq. 15.

$$T_{w,z} = \frac{1}{n}\sum_{i=1}^{n}\left(T_{1,i} - \frac{l_2 \cdot (T_{2,i} - T_{1,i})}{l_1}\right) \tag{15}$$

Thereafter, only heat transfer phenomena in the boiling zone and the evaporation zone of the liquid film are considered.

When vaporizing water at low pressure in the VSPE, for a filling height H_l, the periodic appearance of bubbles is observed at a distance H_b below the free liquid surface [5] such that $H_l > H_b$. And H_b varies according to the operating conditions of each test point. So, the saturation temperature in the boiling zone $T_{sat,z} = T_{sat,b}$ depends on the hydrostatic pressure ($P_{static} = \rho_l g\, d_s$) and the free surface pressure ($P_{sat} = P_{out,ref}$). This saturation temperature is determined by Eq. 16.

$$T_{sat,b} = T_{sat}\left(P_{out,ref} + \rho_l g H_b\right) \tag{16}$$

For the liquid film zone, the saturation temperature $T_{sat,z} = T_{sat,f}$ depends on the free surface pressure ($P_{sat} = P_{out,ref}$) and is determined by Eq. 17.

$$T_{sat,f} = T_{sat}(P_{out,ref}) \tag{17}$$

Thus, the heat transfer coefficient for each zone is determined by Eq. 18.

$$h_z = \frac{\dot{q}_z}{T_{w,z} - T_{sat,z}} \tag{18}$$

The liquid column height (H_l) related to the feed mass flow rate, is calculated by the Eq.19.

$$H_l = \frac{P_{in,ref} - P_{out,ref}}{\rho_l g} \tag{19}$$

The distance between the nucleation site and the free interface (H_b) and the projection height of the droplets forming the liquid film, are determined manually by the software ImageJ. The thermophysical properties of the fluid are calculated according to the saturation temperatures of each medium using Coolprop software.

4. Test of HTC correlations of literature

In order to evaluate the ability of these correlations to predict HTC in the experimental configuration used in this paper, i.e. for confined pool boiling and film liquid evaporation at subatmospheric pressures, a comparison is made between the HTC obtained following the data reduction introduced in 3.4 and the HTC predicted by correlations from the literature. The comparison conducted is: a graphical and statistical comparison conducted by calculating the Mean Absolute Percentage Error (MAE) (Eq. 20), the Mean Relative Percentage Error (MRE) (Eq. 21) and the correlation coefficient (r) (Eq. 22). The MAE is used to check the accuracy of the predictions and the MRE is used to check whether a correlation is over or under predicted average. The percentage of predicted data within a range of ± 30%, noted τ_{30}, is also calculated, to provide a quantitative indication of the correlations performance. This value, although it seems high, is consistent with the very complex phenomena of subatmospheric water boiling [16]. The correlation coefficient, always ranging between -1 and 1, measures the affinity between the experimental and predicted data:

- The closer r is to zero, the weaker the linear relationship.
- Positive values of r indicate a positive correlation when the values of the two variables tend to increase together.
- Negative values of r indicate a negative correlation when the values of one variable tend to increase and the values of the other variable decrease.

- The values 1 and -1 each represent "perfect" correlations, positive and negative respectively. Thus, the relationship is said to be linear.

$$\mathrm{MAE} = \frac{100}{\mathrm{N}} \sum_{\mathrm{i}=1}^{\mathrm{N}} \frac{\left|\mathrm{h}_{\mathrm{pred}} - \mathrm{h}_{\mathrm{exp}}\right|}{\mathrm{h}_{\mathrm{exp}}} \tag{20}$$

$$\mathrm{MRE} = \frac{100}{\mathrm{N}} \sum_{\mathrm{i}=1}^{\mathrm{N}} \left(\frac{\mathrm{h}_{\mathrm{pred}} - \mathrm{h}_{\mathrm{exp}}}{\mathrm{h}_{\mathrm{exp}}}\right) \tag{21}$$

$$r = \frac{cov\ (\mathrm{h}_{\mathrm{exp}}, \mathrm{h}_{\mathrm{pred}})}{\sqrt{var(\mathrm{h}_{\mathrm{exp}}) \cdot var(\mathrm{h}_{\mathrm{pred}})}} \tag{22}$$

To remain consistent, the constant (C) and coefficient (a and b) of the correlation Eq. (1) are fitted to the experimental database of Giraud et al. [16] (Table 3), minimising the sum of the differences between the experimental and theoretical values of the Nusselt number (Nu). The parameters constituting Eq. 1 are calculated as a function of the saturation temperatures of each medium considered. The definition of the carateritic length (δ) and velocity (U) depends on the area under consideration (table 7).

Table 3 : Constants and coefficients fitted to experimental database of Giraud et al. [16]

Constants and coefficients fitted			
C	**a**	**b**	**Zones**
38.405	0.484	−1.976	Pooling boiling
0.067	0.742	−1.541	Liquid film evaporation

4.1. Pool boiling zone

The results of the comparisons between the experimental HTC of pool boiling and those predicted by the literature correlations are shown to the Fig. **5** (graphical comparison) and Table **4** (statistical comparison).

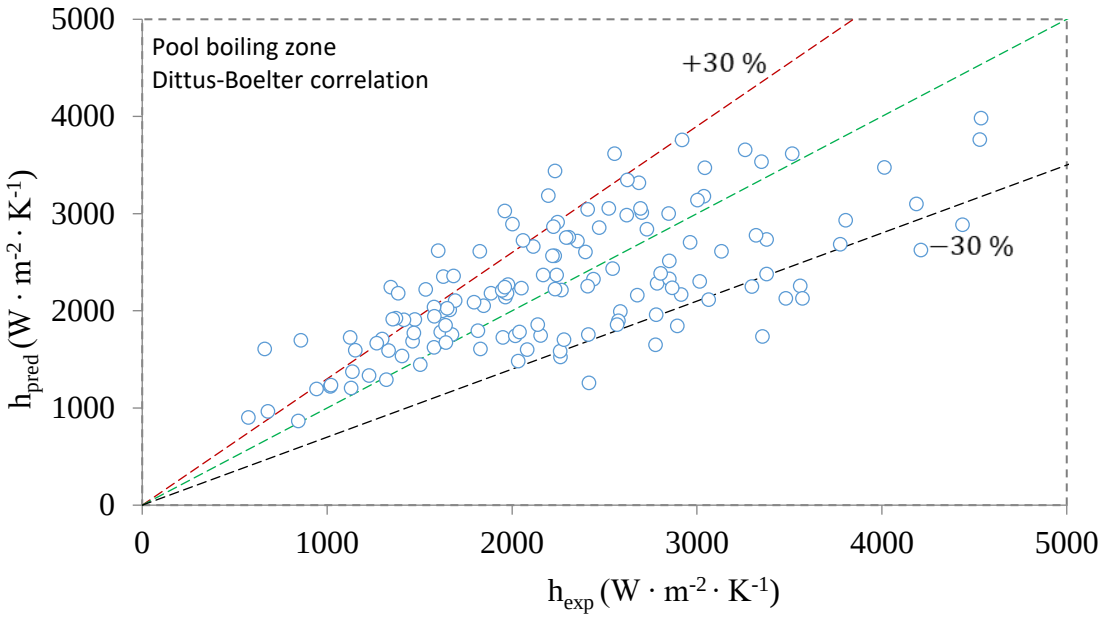
Pool boiling zone
Dittus-Boelter correlation
+30 %
−30 %
5000
4000
3000
2000
1000
0
0
1000
2000
3000
4000
5000
h_{pred} (W · m^{-2} · K^{-1})
h_{exp} (W · m^{-2} · K^{-1})

(a)

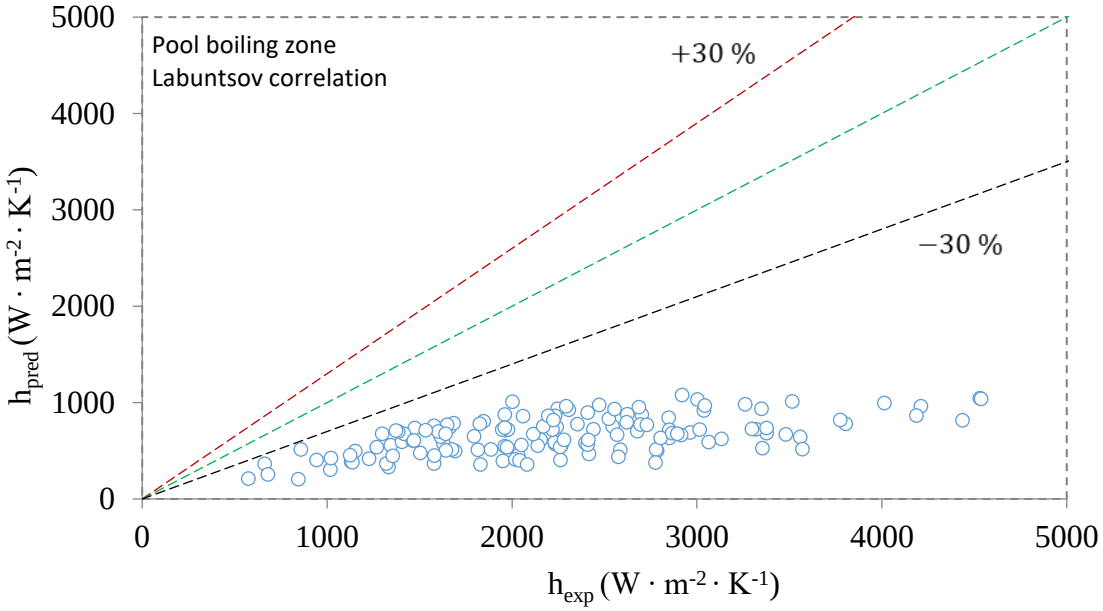
Pool boiling zone
Labuntsov correlation
+30 %
−30 %
5000
4000
3000
2000
1000
0
0
1000
2000
3000
4000
5000
h_{pred} (W · m^{-2} · K^{-1})
h_{exp} (W · m^{-2} · K^{-1})

(b)

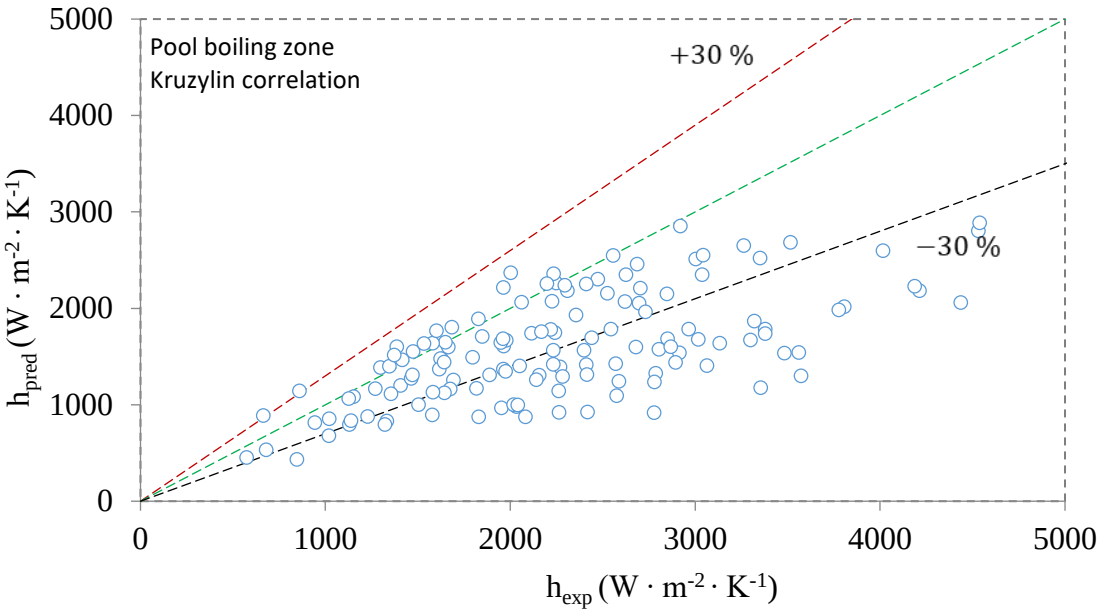
Pool boiling zone
Kruzylin correlation
+30 %
−30 %
5000
4000
3000
2000
1000
0
0
1000
2000
3000
4000
5000
h_{pred} (W · m^{-2} · K^{-1})
h_{exp} (W · m^{-2} · K^{-1})

(c)

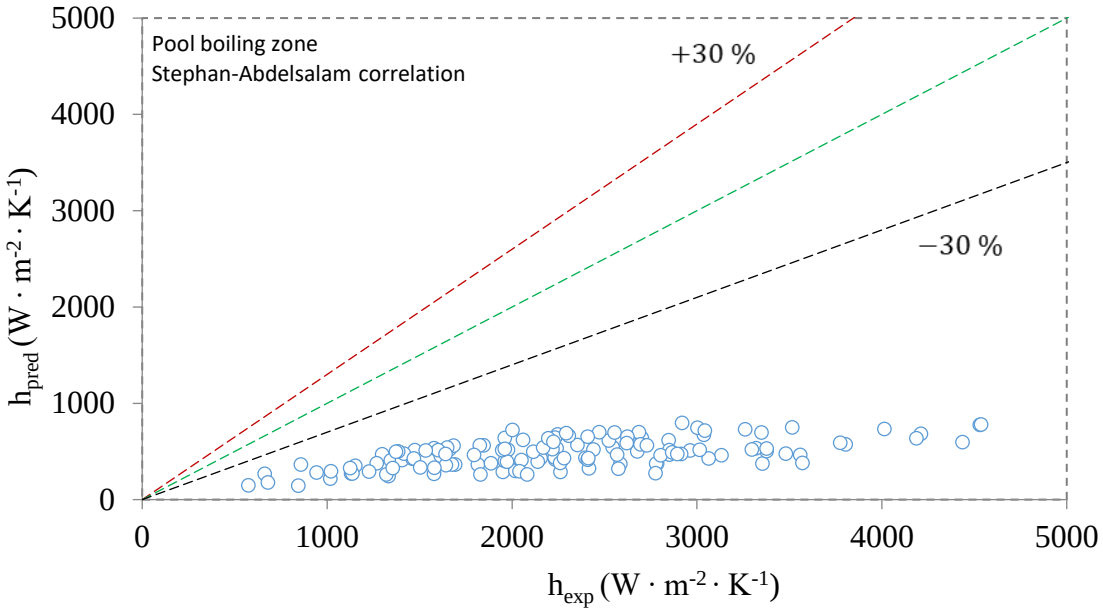
Pool boiling zone
Stephan-Abdelsalam correlation
+30 %
−30 %
5000
4000
3000
2000
1000
0
0
1000
2000
3000
4000
5000
h_{pred} (W · m^{-2} · K^{-1})
h_{exp} (W · m^{-2} · K^{-1})

(d)

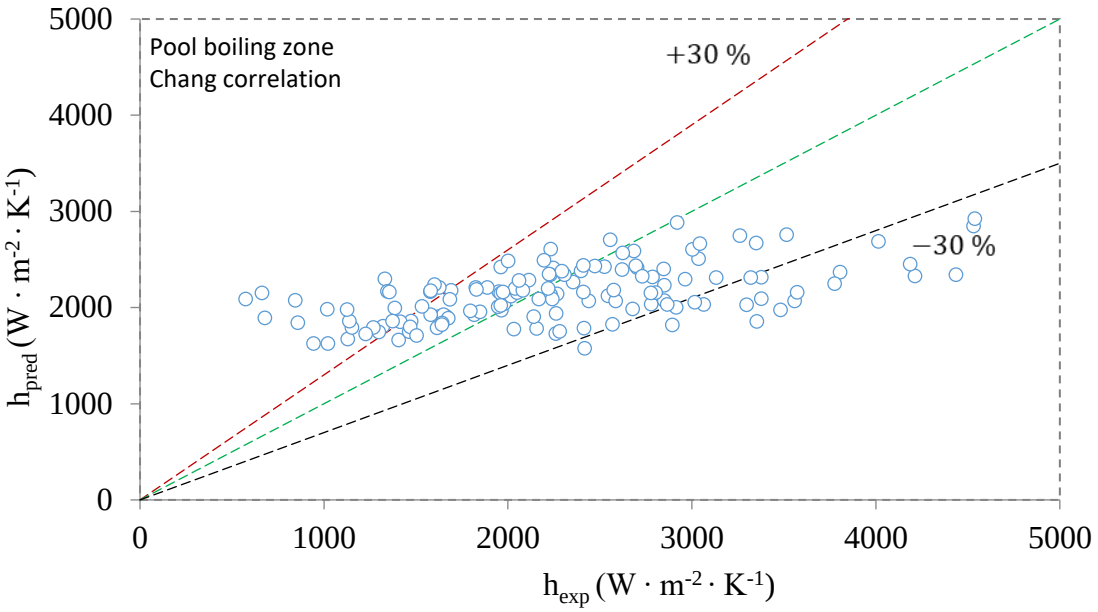
Pool boiling zone
Chang correlation
+30 %
−30 %
5000
4000
3000
2000
1000
0
0
1000
2000
3000
4000
5000
h_{pred} (W · m^{-2} · K^{-1})
h_{exp} (W · m^{-2} · K^{-1})

(e)

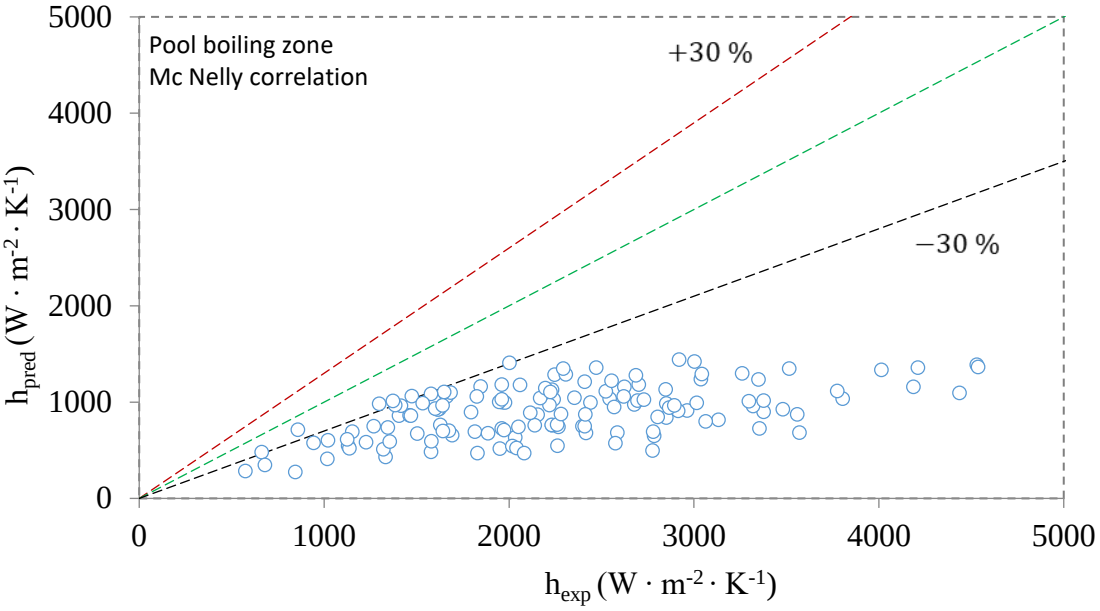
Pool boiling zone
Mc Nelly correlation
+30 %
−30 %
5000
4000
3000
2000
1000
0
0
1000
2000
3000
4000
5000
h_{pred} (W · m^{-2} · K^{-1})
h_{exp} (W · m^{-2} · K^{-1})

(f)

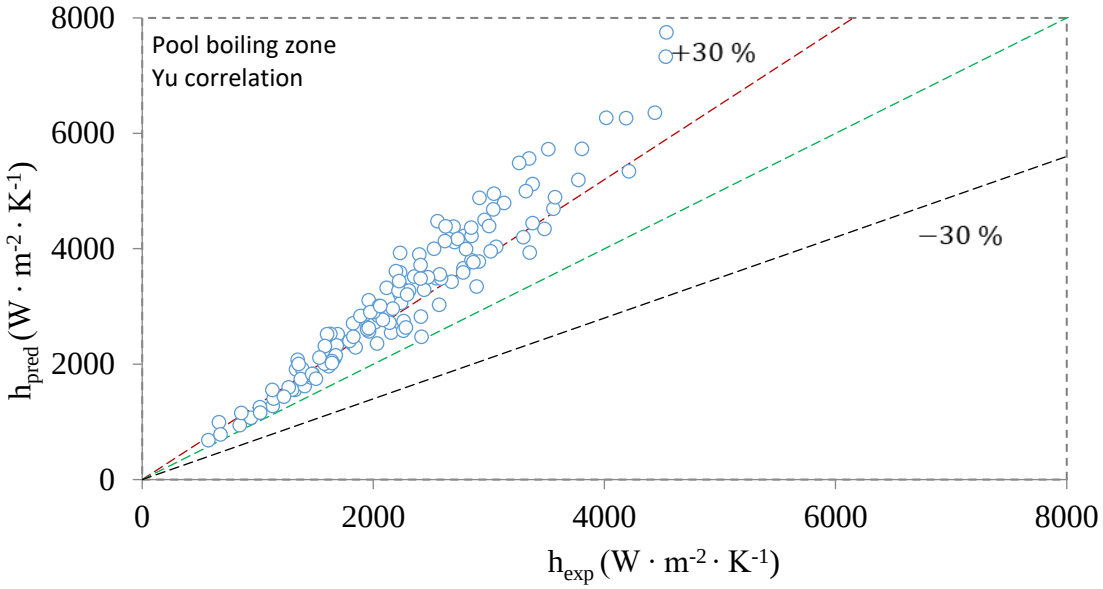

(g)

Figure 5 : Comparison between experimental HTC (h_{exp}) of pool boiling zone and HTC predicted (h_{pred}) by correlations of: (a) Dittus-Boelter [19], (b) Labuntsov [11], (c) Kruzylin [11], (d) Stephan-Abdelsalam [11], (e) Chang [13], (f) Mc Nelly [21] and (g) Yu [20]

Table 4 : Statistical comparison between the HTC experimental of pool boiling zone and the HTC predicted by the correlations in the literature.

	Pool boiling zone			
Correlations	MAE [%]	MRE [%]	τ_{30}[%]	r [−]
Dittus-Boelter [19]	24	7	73	0.67
Kruzylin [11]	28	− 26	54	0.64
Labuntsov [11]	69	− 69	0	0.58
Stephan-Abdelsalam [11]	77	− 77	0	0.60
Chang [13]	29	8	69	0.57
Mc Nelly [21]	57	− 57	3	0.55
Yu [20]	39	39	27	0.96

Table 4 indicates that the HTC experimental database for the pool boiling area did not accurately match the majority of the correlations considered.

Labuntsov (Eq.2) and Stephan-Abdelsalam (Eq. 4) correlations show the worst results by predicting 0% of the experimental database within an error band of ±30%. Mc Nelly (Eq. 9) and Yu (Eq. 10) correlations, also poorly predict 3%, and 27% of the experimental database within an error band of ±30%, respectively. All these above-mentioned correlations give very poor precision and underestimate the experimental database. The Dittus-Boelter (Eq. 1), Kruzylin (Eq. 3) and Chang (Eq. 6) correlations, however, provided more accurate results. Dittus-Boelter correlation shows the best performance by satisfactory predicts 73 % of the database within an error band of ±30% with an accuracy of 24%. For the pool boiling zone, this correlation over-estimates the experimental values by 7%. Kruzylin correlation correctly predicts 54 % of the database within a ±30% error band with an accuracy of 28%. The correlation (Eq. 3) underpredicts 26% of the experimental data. Chang correlation offers a

satisfactory result and correctly predicts 69% of the database within an error band of ±30% with an accuracy of 29 %. It over-estimates the experimental values by 8 %.

4.2. Liquid film evaporation zone

For the liquid film evaporation zone, the comparison between the experimental HTC and those estimated by correlations from the litterature are shown in the Fig. 6 (graphical comparison) and Table 5 (statistical comparison).

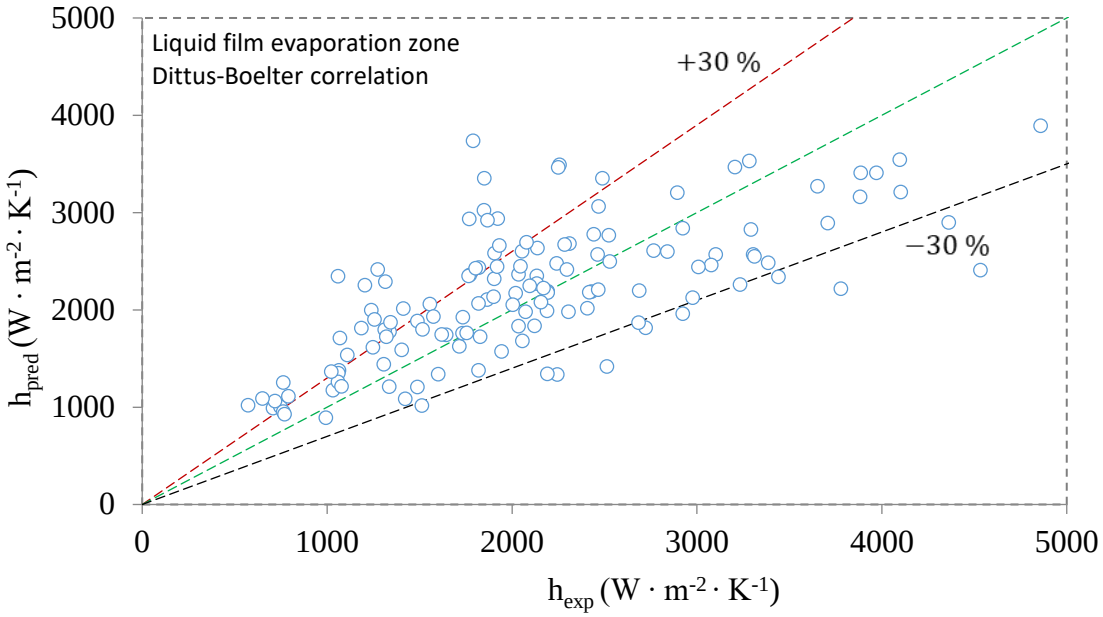

(h)

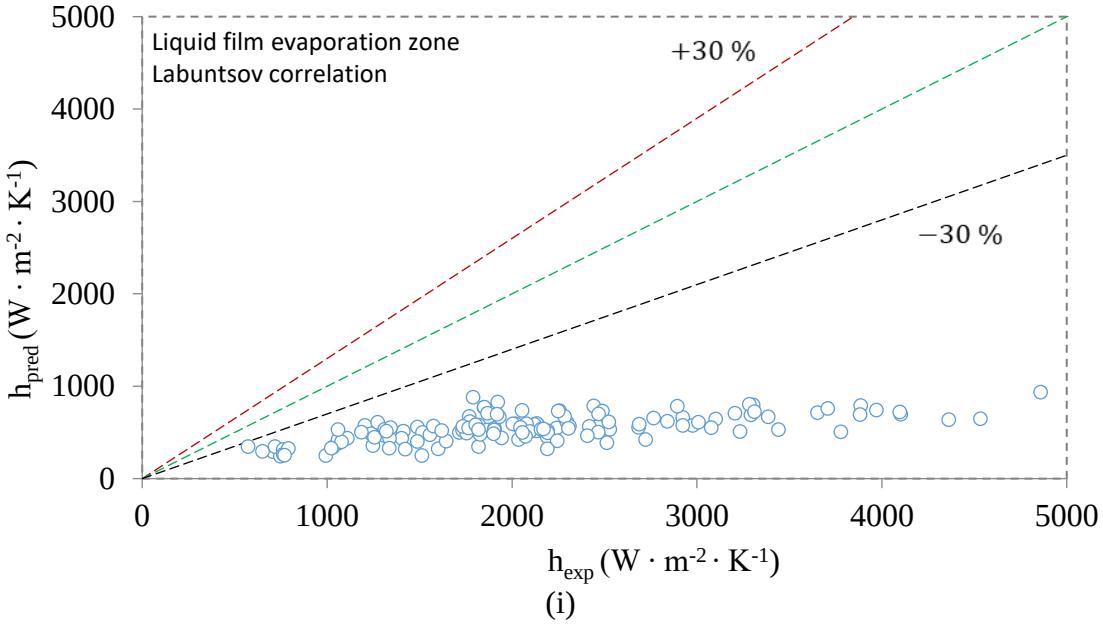

(i)

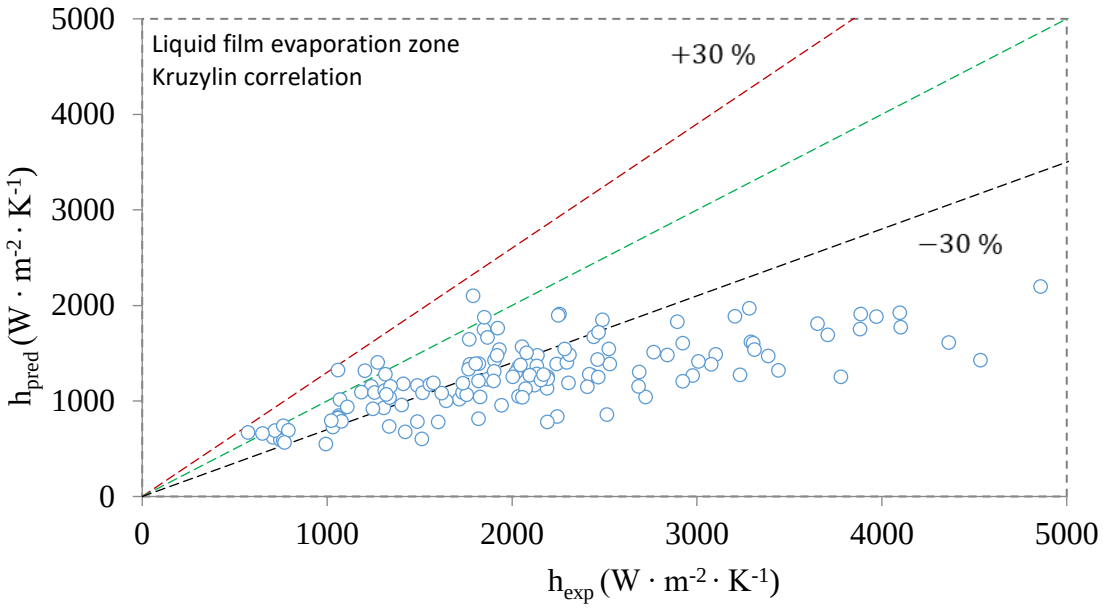
Liquid film evaporation zone
Kruzylin correlation
+30 %
−30 %
5000
4000
3000
2000
1000
0
0
1000
2000
3000
4000
5000
h_{pred} (W · m^{-2} · K^{-1})
h_{exp} (W · m^{-2} · K^{-1})

(j)

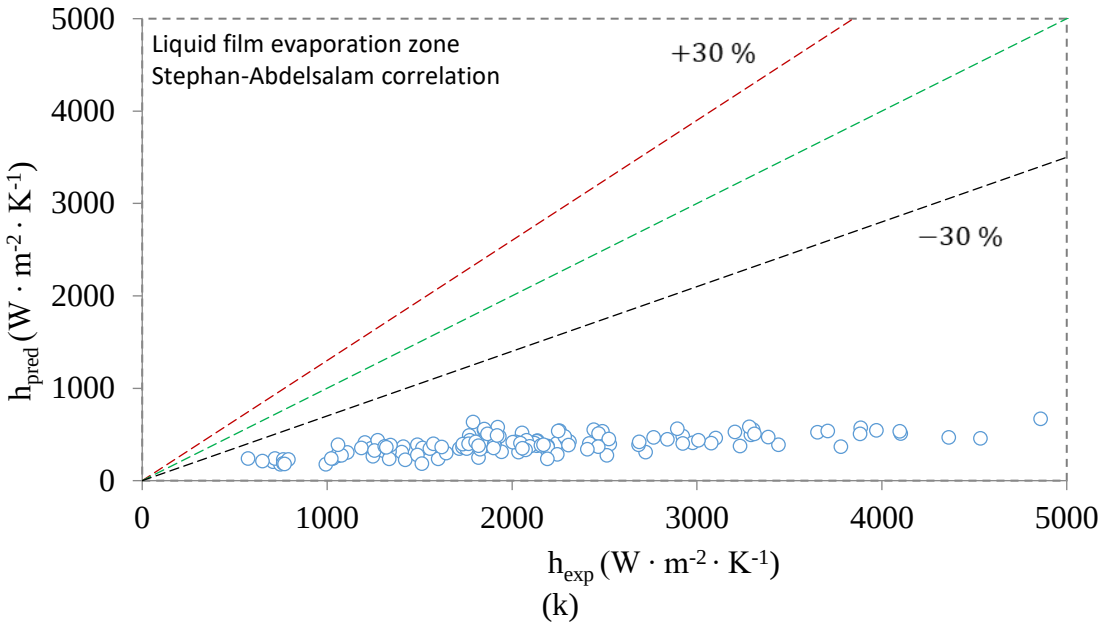
Liquid film evaporation zone
Stephan-Abdelsalam correlation
+30 %
−30 %
5000
4000
3000
2000
1000
0
0
1000
2000
3000
4000
5000
h_{pred} (W · m^{-2} · K^{-1})
h_{exp} (W · m^{-2} · K^{-1})

(k)

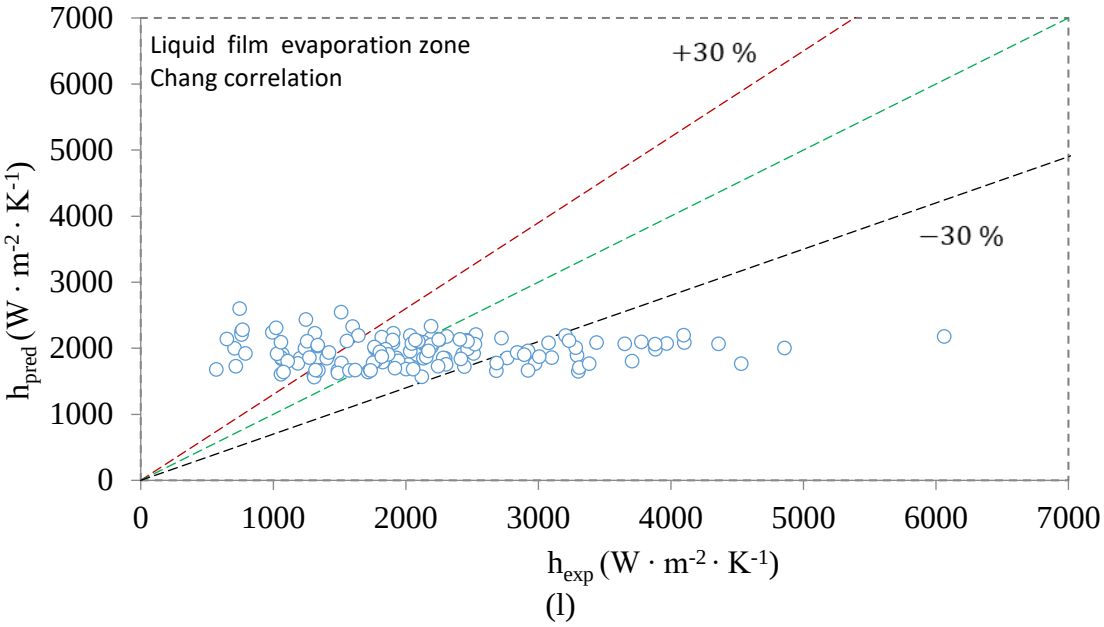
Liquid film evaporation zone
Chang correlation
+30 %
−30 %
7000
6000
5000
4000
3000
2000
1000
0
0
1000
2000
3000
4000
5000
6000
7000
h_{pred} (W · m^{-2} · K^{-1})
h_{exp} (W · m^{-2} · K^{-1})

(l)

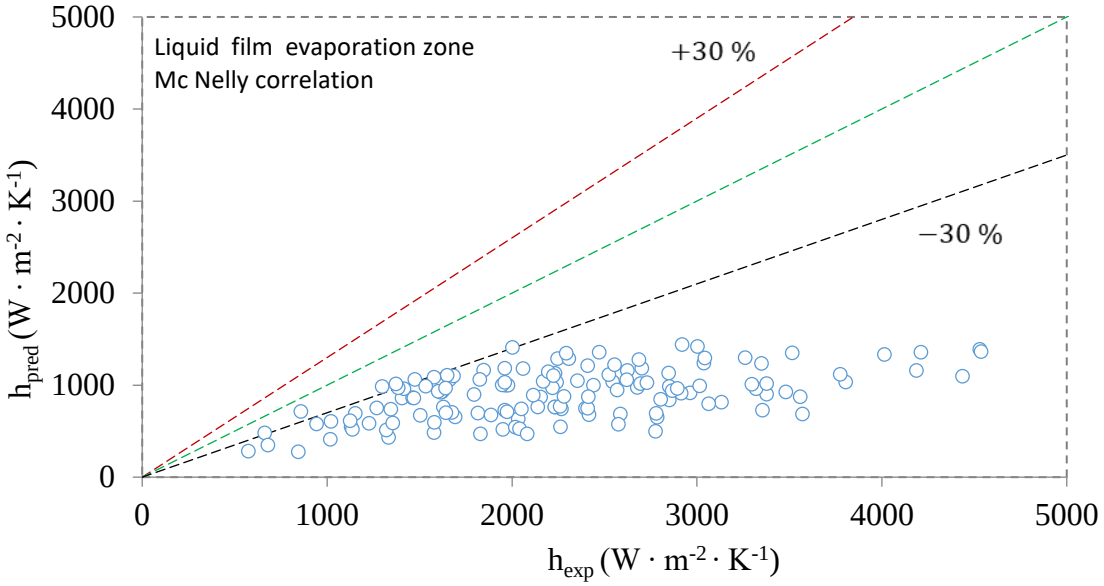
Liquid film evaporation zone
Mc Nelly correlation
+30 %
−30 %
5000
4000
3000
2000
1000
0
0
1000
2000
3000
4000
5000
h_{pred} (W · m^{-2} · K^{-1})
h_{exp} (W · m^{-2} · K^{-1})

(m)

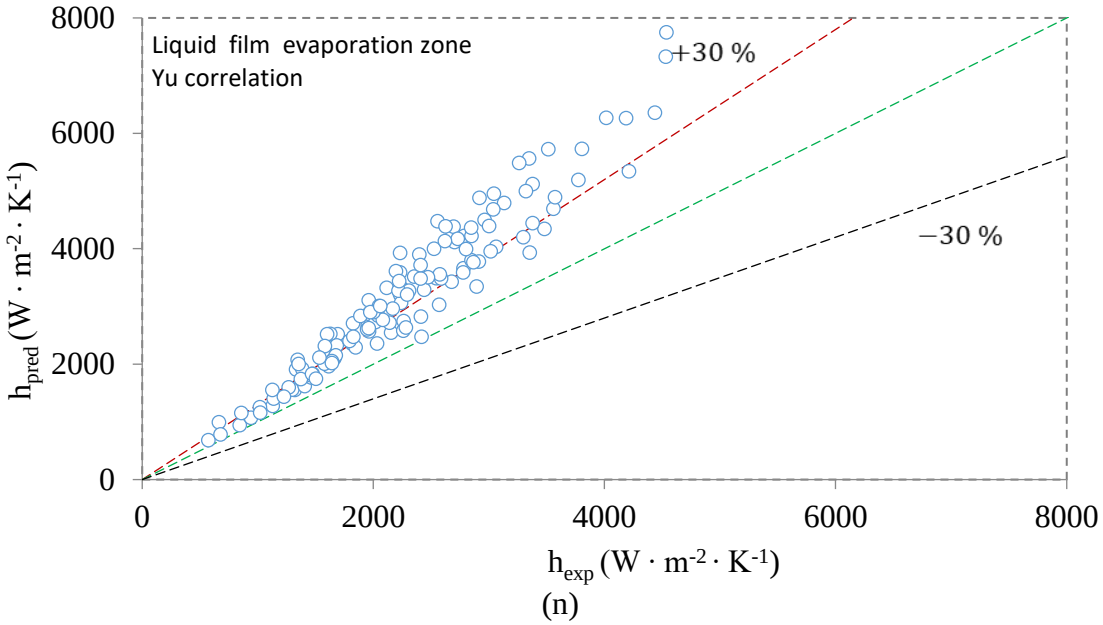

(n)

Figure 6 : Comparison between experimental HTC (h_{exp}) of liquid film evaporation zone and HTC predicted (h_{pred}) by correlations of: (h) Dittus-Boelter [19], (i) Labuntsov [11], (j) Kruzylin [11], (k) Stephan-Abdelsalam [11], (l) Chang [13], (m) Mc Nelly [21] and (n) Yu [20]

Table 5 : Statistical comparison between the experimental HTC of liquid film evaporation zone and the HTC predicted by the correlations from the literature

	Liquid film evaporation zone			
Correlations	MAE [%]	MRE [%]	τ_{30}[%]	r
Dittus-Boelter [19]	27	12	68	0.72
Kruzylin [11]	36	− 34	35	0.72
Labuntsov [11]	73	− 73	0	0.67
Stephan-Abdelsalam [11]	80	− 80	0	0.69
Chang [13]	40	13	54	0.50
Mc Nelly [21]	61	− 61	1	0.64
Yu [20]	31	31	45	0.97

Table **5** shows that correlations from the literature do not accurately predict the experimental HTC database for the liquid film evaporation zone, despite their validity at low-pressure conditions and/or the amount and diversity of involved parameters in their development.

Labuntsov (Eq. 2) and Stephan-Abdelsalam (Eq. 4) correlations show the worst results by predicting 0 % of the experimental database within a ±30% error band. As for the Kruzylin (Eq. 3), Mc Nelly (Eq. 9) and Yu (Eq. 10) correlations, they also poorly perform by predicting 35%, 1% and 45% respectively of the experimental database within a ±30% error band. However, Dittus-Boelter (Eq. 1) and Chang (Eq. 6) correlations provided satisfactory results. Dittus-Boelter correlation (Eq. 1) correctly predicts 68 % of the database within an error band of ± 30% with an accuracy of 27%. It over-estimates the experimental values by 12%. Chang correlation (Eq. 7) correctly predicts 54% of the database within a ±30% error band with an

accuracy of 40%. The values calculated with the correlation (Eq. 7) are increased by 13% compared to the experimental values.

The poor results of the correlations from the litterature in accurately predicting the heat transfer coefficient may be due to the complexity of the coupled mechanisms involved during confined vaporization at subatmospheric pressure. Furthermore, with the exception of the correlations (Eq. 6) and (Eq. 7), the other correlations were originally designed to predict free boiling heat transfer coefficients and at higher pressures, although their validity at low pressures has been verified by [11] [21] and [20]. All these correlations are also developed for higher heat flux densities than those observed in this study. From a physical point of view, the observations of Chang et al. [13] are in perfect agreement with those observed by Giraud et al. [5] [16]. Therefore, the good performance of the correlations (Eq. 6) and (Eq. 7) was expected.

However, all these correlations in the literature (Eq. 1 to Eq. 10, except Eq. 5) do not take into account all the relevant parameters that influence the HTC at low pressure. For example, the liquid height is absent of these equations whereas it has been shown that this parameter strongly influence the heat transfer at low pressure [13] [4] [14] [24] [15]. Also, given the centimetric size of the bubbles during the vaporization of water at subatmospheric pressure [4] , a parameter influencing their rise and their growth would obviously be determining. It should also be noted that the dimensional analysis adopted for the development of the correlations (Eq. 1 to Eq. 10, except Eq. 5), does not verify the physical independence of the physical quantities. For the correlations of Labuntsov (Eq. 2), Kruzylin (Eq. 3), Stephan-Abdelsalam (Eq. 4), Chang (Eq. 6 and Eq. 7), Mc Nelly (Eq.9) and Yu (Eq. 10), the thermophysical properties of the fluid and the heat flux density ($\dot{q}$), depend on the saturation conditions of the medium (P_{sat}, T_{sat}). Eq. 5 also shows a dependence between the bubble diameter (d_b) and the thermophysical properties of the fluid. However, it is necessary to ensure that no physical quantity, apart from the variable of interest, depends on the variation of the other quantities [18]. This independence is a key factor for modeling by dimensional analysis since it makes possible to easily transpose results from one scale to another (similarity).

5. New pool boiling and liquid film evaporation HTC predictive correlations

5.1. Dimensional analysis

Based on the scientific knowledge generated by the literature, the rigorous dimensional analysis approach based on the Vaschy-Buckingham theorem requires the definition of the independent physical quantities governing the heat transfer phenomena occurring in the evaporator (Fig.2a). These parameters, which are to be considered during boiling and evaporation at subatmospheric pressures in the evaporator, are the thermophysical properties of the liquid and vapour, the thermodynamic conditions (pressure and temperature) and boundary conditions.

The HTC (h) on the refrigerant side, the target variable or variable of interest, depends mainly on : the pressure (P_{sat}), the vapor mass velocity (G_v), the heat flow ($\dot{q}$), the enthalpy of change of state from liquid to vapour (Δh_{lv}) , the difference between the refrigerant side wall temperature T_w and the temperature of the saturated liquid medium T_{sat} noted (ΔT) (maximum temperature difference for a bubble to develop), the densities of the liquid and vapour (ρ_l and ρ_v), the vapour density at liquid temperature (ρ_b), the specific heat (or mass heat capacity) of the liquid (c_{p_l}), the thermal conductivity of the liquid (λ_l), the dynamic viscosities of the liquid

and vapor (μ_l and μ_v), the surface tension at the liquid-vapour interface (σ), the thickness of the plate containment (e), the liquid column height (H_l), and the acceleration of gravity (g).

The crucial point for a rigorous dimensional analysis is the verification of the physical independence of the listed physical quantities. It is then necessary to make sure that no physical quantity, except the variable of interest h, is influenced by the variation of the other quantities [18]. All the thermophysical properties of the refrigerant, listed here, except the vapour density at liquid temperature (ρ_b), are physically dependent on the saturation conditions of the medium (P_{sat}, T_{sat}). The vapor mass velocity is defined by Eq. 23 which shows that G_v, Δh_{lv}, and $\dot{q}(\Delta T)$ do not have to be listed simultaneously. It is then sufficient to take one of these parameters (for example: G_v).

$$G_v = \frac{\dot{q}_z}{\Delta h_{lv}} \tag{23}$$

Thus, the problem can be set as follows:

$$h = h\left(H_l, \mu_v, \rho_v, \rho_b, \sigma, g, \lambda_l, G_v, e, \mu_l, \rho_l, c_{p_l}\right) \tag{24}$$

The mathematical model of the physical law studied (Eq. 24) indicates that the HTC (h) depends on 12 independent dimensional parameters. Thus, the Vaschy-Buckingham theorem allows us to express Eq. 24 in dimensionless form by Eq. 25 (see details in Appendix A).

$$Nu = Nu(F^*, \mu^*, \rho^*, \rho_v^*, Bo, Ca, Pr, We) \tag{25}$$

Thus, Eq. 25 shows that the Nusselt number (Nu) depends on 8 dimensionless groups. Since the heat transfer phenomena in the pool boiling zone and the evaporation zone of the liquid film observed (Fig. 3), are considered, the thermophysical properties of the fluid vary according to each medium as they are calculated according to the saturation temperatures defined by Eq. 16 and Eq.17. Although the physical meaning and/or definition of the dimensionless numbers introduced in Eq. 25 may depend on the area considered (pool boiling or liquid film evaporation), the formulation for each area remains identical. The definition of these and their meaning are described in Table 6.

Table 6 : Dimensionless numbers

Notations	Formulas	Physical definitions and meaning
Nu	$\frac{h\,\delta}{\lambda_l}$	Nusselt number compares the effective thermal energy transport through the boundary layer between the refrigerant and the core plate wall (convective transfer) to purely diffusive conduction (conduction in the medium).
F^*	$\frac{e}{H_l}$	The form factor is the ratio between the plate confining thickness (e) and the water column height (H_l) .It allows to find the right filling ratio and channel thickness for better system performance and is thus of great importance for the evaporator sizing.

ρ_v^*	$\frac{\rho_b}{\rho_v}$	The ratio between the density of vapour at liquid temperature (ρ_b) and the density of vapour at saturation temperature (ρ_v) is a determining parameter that influences the rise and growth of bubbles at low pressure.
F^{**}	$\frac{e}{\delta}$	The shape factor is the ratio between the containment thickness of the plate (e) and the characteristic length (δ).
Ca	$\frac{U\,\mu_l}{\sigma}$	Capillary number compares the force of viscosity to the force of interfacial tension (e.g., two-phase microchannel flow).
We	$\frac{\rho_l\ U^2\ \delta}{\sigma}$	Weber number characterizes the flow of fluids at the interface of a multiphase system. It corresponds to the ratio of inertial forces to surface tension forces.

516

517 The definition of the characteristic length (δ) and velocitie (U) depends on the area
518 considered. The physical quantities that constitute them are different whether the pool boiling
519 zone or the falling film zone is considered. These numbers are defined in table 7.

Table 7 : characteristic lengths (δ) and velocities (U)

Notations	Formulas	Physical definitions and meaning	Zones
$\delta = \delta_b$	$\sqrt{\frac{\sigma}{\rho_l\, g}}$	δ_b is the modified capillary length. It is the characteristic distance below which capillary phenomena are predominant over gravitational phenomena. The modified capillary length characterizes the relationship between the surface tension forces and the gravitational forces acting on the interface.	Pool boiling
$U = U_b$	$\frac{\dot{q}_b}{\rho_v\, \Delta h_{lv}}$	U_b is the superficial velocity of the vapour bubble.	Pool boiling
$\delta = \delta_f$	$\left(\frac{\mu_l^2}{\rho_l^2\, g}\right)^{\frac{1}{3}}$	δ_f is the visco-gravity length.	Liquid film evaporation
$U = U_f$	$\frac{\dot{q}_f}{\rho_v\, \Delta h_{lv}}$	U_f is the characteristic average evaporation velocity of the liquid film, determined on the basis of the total heat flux at the wall.	Liquid film evaporation

520

521 Thus, for the pool boiling zone, F^{**} (Table **6**) is the Bond number (Bo). It represents the
522 ratio of buoyancy forces to surface tension forces. It is commonly used in confined boiling
523 studies and can be seen as an indicator of bubble "squeezing" [25].

524 For the falling film zone, F^{**} (Table **6**) is the shape factor between the containment
525 thickness of the plate (e) and visco-gravity length (δ_f) (noted Bo_f) since the flow of the liquid
526 film falling on the vertical smooth plate (Fig.2) is induced by the gravity force (gravity flow).
527 The thickness of the liquid film necessarily depends on the visco-gravity length and the flow

528 velocity. The HTC during evaporation of a liquid film running down a wall depends on the
529 thickness of the film, which depends on the flow regime.

530 **5.2. Development of news HTC correlations**

531 The monomial form (Eq. 26) was preferred to simplify the identification of the
532 unknowns. Indeed, the relatively general form, i.e., the one based on a sum of monomials where
533 each monomial is a product of internal measurements at different powers, more accurate, makes
534 the identification of the unknowns very complex and requires a lot of experimental data.
535 Moreover, in the search for the process relationship via a monomial form, it is necessary to rely
536 on an experimental program where each of the dimensionless numbers varies within a
537 sufficiently wide range. Otherwise, the value of the exponents $a_{i\in[1;8]}$ is not guaranteed and
538 may bias the value of the constant C [18].

$$\mathrm{Nu} = \mathrm{C} \cdot (\mathrm{F}^*)^{a_1} \cdot (\mu^*)^{a_2} \cdot (\rho^*)^{a_3} \cdot (\rho_v^*)^{a_4} \cdot (\mathrm{Bo})^{a_5} \cdot (\mathrm{Ca})^{a_6} \cdot (\mathrm{Pr})^{a_7} \cdot (\mathrm{We})^{a_8} \quad (26)$$

539

540 For the range of operating points tested in this study, the dimensionless numbers
541 μ^*, ρ^* and Pr show small variations that bias the values of coefficients and the constant C of
542 Eq. 26. As a result, their elimination from the list of thermophysical properties is possible and
543 this does not change the appearance of the scatterplot cloud formed by Eq. 26. This elimination
544 is in line with the suggestion of Kew and Corwell (1997) quoted by [26], who encourages to
545 eliminate any non-dimensional group that does not improve the accuracy of the prediction
546 model. However, there is no evidence that the non-dimensional group eliminated do not
547 improve the accuracy of the model prediction in another range of operating conditions and/or
548 with another fluid. Thus, in this paper Eq. 26 is simplified by becoming the Eq. 27 but it is
549 highly recommended to use Eq. 26 for higher variation of μ^*, ρ^* and Pr.

$$\mathrm{Nu} = \mathrm{C} \cdot (\mathrm{F}^*)^{a_1} \cdot (\rho_v^*)^{a_2} \cdot (\mathrm{F}^{**})^{a_3} \cdot (\mathrm{Ca})^{a_4} \cdot (\mathrm{We})^{a_5} \quad (27)$$

550

551 Based on the regression analysis of the experimental database, using the least squares
552 method (minimizing the sum of the differences between the experimental and theoretical values
553 of the Nusselt number Nu), following HTC correlations is obtained:

554 - **Pool boiling zone**

$$\frac{h\,\delta_b}{\lambda_l} = 2.664 \cdot 10^{-6} \cdot \left(\frac{e}{H_l}\right)^{0.410} \cdot \left(\frac{\rho_b}{\rho_v}\right)^{0.157} \cdot \left(\frac{e}{\delta_b}\right)^{-0.382} \cdot \left(\frac{U_b\,\mu_l}{\sigma}\right)^{-2.812} \cdot \left(\frac{\rho_l\,U_b^2\,\delta_s}{\sigma}\right)^{1.630} \quad (28)$$

555

556 - **Liquid film evaporation zone**

$$\frac{h\,\delta_f}{\lambda_l} = 1.195 \cdot 10^{-8} \cdot \left(\frac{e}{H_l}\right)^{-0.411} \cdot \left(\frac{\rho_b}{\rho_v}\right)^{0.231} \cdot \left(\frac{e}{\delta_f}\right)^{0.767} \cdot \left(\frac{U_f\,\mu_l}{\sigma}\right)^{-3.247} \cdot \left(\frac{\rho_l\,U_v^2\,\delta_f}{\sigma}\right)^{1.929} \quad (29)$$

557

558 The domain of correlations application is the important factor that limits its
559 performance. The correlations Eq. (28) and Eq. (29) are developed according to the range
560 covered by the experimental test (Table 1). Thus, for working pressures ranging from 0.7 to
561 1.8 kPa, and for dimensionless numbers which vary according to the ranges listed in Table 8.
562 The heat fluxes and superheats that allowed the determination of the experimental HTC (Eq.
563 18) are between 1352-14507 $\mathrm{W.m^{-2}}$ and 1.12-7.14 K respectively.

Table 8 : Dimensionless numbers range of variation

(a) Pool boiling	
Dimensionless numbers	**Validity range**
Nusselt number, Nu	$2.751 \leq \ Nu \leq 21.118$
Form factor, F^*	$0.007 \leq \ F^* \leq 0.106$
Vapor density ratio, ρ_v^*	$1.259 \leq \ \rho_v^* \leq 2.507$
Capillary number, Ca	$0.001 \leq \ Ca \leq 0.013$
Bond number, Bo	$0.722 \leq \ Bo \leq 2.192$
Weber number, We	$0.164 \leq \ We \leq 16.948$
(b) Liquid film evaporation	
Nusselt number, Nu	$0.064 \leq \ Nu \leq 0.530$
Form factor, F^*	$0.007 \leq \ F^* \leq 0.106$
Vapor density ratio, ρ_v^*	$1.332 \leq \ \rho_v^* \leq 2.524$
Capillary number, Ca	$0.001 \leq \ Ca \leq 0.016$
Modified Bond number, Bo_f	$31.111 \leq \ Bo_f \leq 117.917$
Weber number, We	$0.002 \leq \ We \leq 0.479$

Eq. (28) and (29) show opposite sign exponents for the dimensionless group $\frac{e}{H_l}$ in one hand (positive sign for the pool boiling zone, negative sign for the liquid film evaporation zone) and $\frac{e}{\delta_{f/b}}$ on the other hand (negative sign for the pool boiling zone, positive sign for the liquid film evaporation zone). Although the obtained values of the exponents have no physical meaning since they are obtained by a mathematical fitting, the obtained opposite sign could be expected. Indeed, for a given thickness of the narrow channel, low H_l leads to relative high bubble frequency. Since the bubble frequency is high, the liquid film created by these bubbles is often regenerated leading to thicker falling film. On the contrary, high H_l leads to low bubble event and the falling film could get thinner before being regenerated again. Thus, the estimated HTC is expected to be higher in the pool boiling zone for low H_l than for high H_l values, whereas in the falling film evaporation zone, the reverse trend is expected: a higher HTC is expected for high H_l than low H_l. Regarding the dimensionless group $\frac{e}{\delta_{f/b}}$, the physical meaning is different regarding the considered zone. Indeed, in the pool boiling zone, $\delta_b$refers to the capillary length whereas in the liquid film zone δ_f refers to the visco-gravity length. Nevertheless, the obtained sign could be explained by the fact that, for a given running conditions, a lower e leads to a warmer environment fostering boiling in on hand whereas it increases friction and refrains the falling of the liquid film in the other hand.

6. Evaluation and validation of the developed correlations

Fig. 7 a and b reflect the graphical comparisons between the experimental HTC and the HTC calculated by the correlations (Eq. 28) and (Eq. 29) (named thereafter “new correlation”).

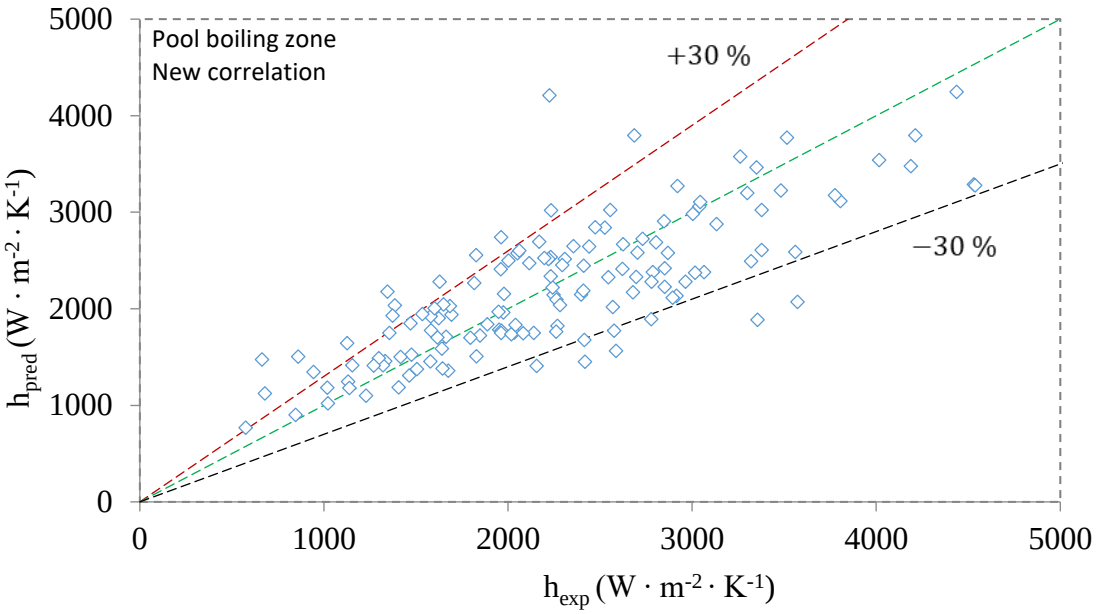

(a)

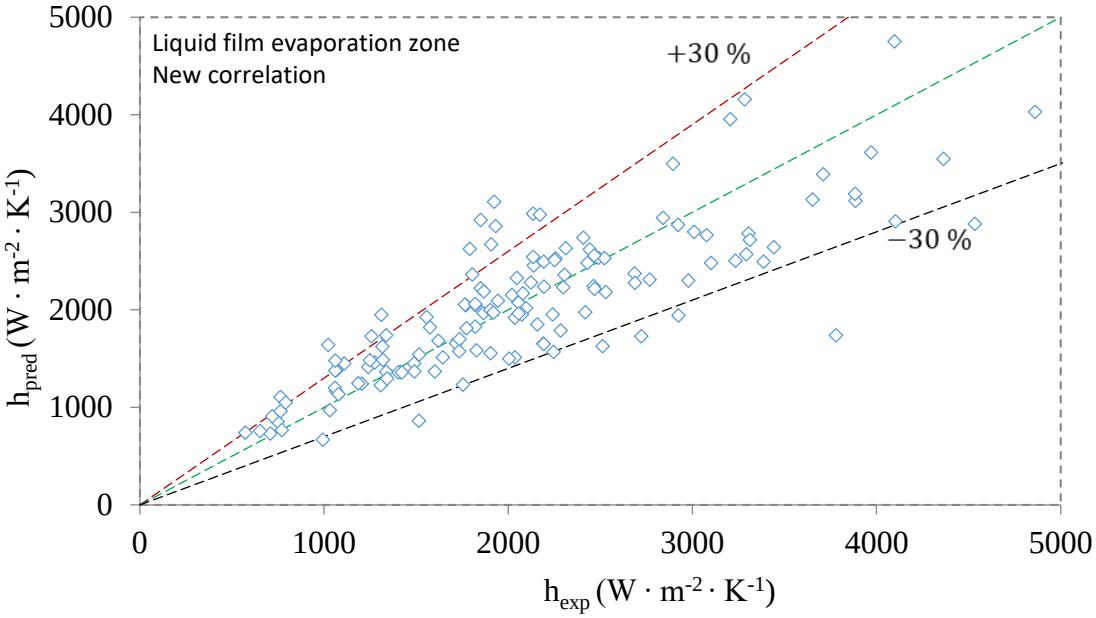

(b)

Figure 7 : Comparison between the experimental HTC (h_{exp}) and the HTC calculated (h_{pred}) by the new correlations: (a) pool boiling zone, (b) liquid film evaporation zone.

The quantitative indications of the performance of the developed correlations (Eq. 28 and Eq. 29) are the following: they predict 86 % (MRE = 3 % and MAE = 19 %) and 83 % (MRE = 2 % and MAE = 18 %), respectively, of the experimental database within an error band of ±30%. The correlation coefficients of Eq. 28 and Eq. 29 are respectively equal to 0.79 and 0.84 and the shape of the scatterplots (Fig. 7 a and b) show that the experimental and predicted heat transfer coefficients are strongly linearly correlated. Thus, they very satisfactory results. From a physical point of view, the new models involve different dimensionless numbers of great importance for the sizing of two-phase heat exchangers (Table **6**). For example, the form

factor (e/H_l) should help in finding the right filling ratio and channel thickness to obtain the best system performance. They are then made up of dimensionless numbers that have a physical meaning and relevance to the phenomenon being studied. However, a predictive correlation must not only have reasonable statistical similarity to the experimental results, but it must also capture trends in the experimental data. Thus, Fig. 8 represents the variations of the calculated HTC (h_{pred}) by the newly proposed correlations as a function of the heat fluxes ($\dot{q}$), at fixed pressures (P_{sat}).

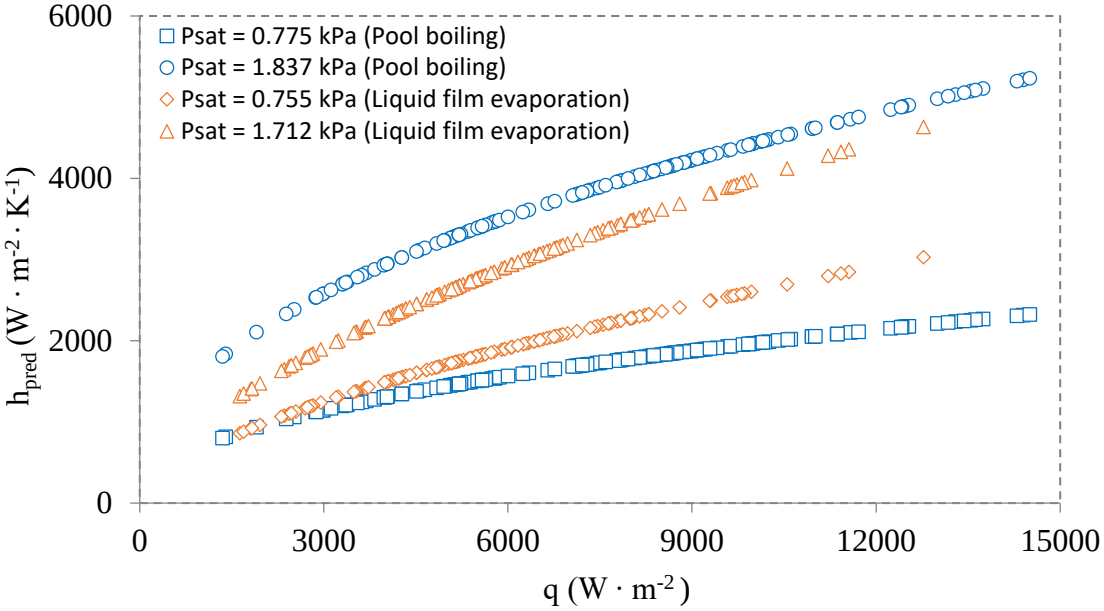

Figure 8 : Variations of HTC predicted by the proposed new correlations as a function of heat flux

According to Fig. 8, at each given P_{sat}, h_{pred} increases with heat flux (q). That is, when q and/or P_{sat} increase, h_{pred} increases accordingly. In other words, at subatmospheric pressure, when the heat flux is constant, the water pool boiling or liquid film evaporation HTC increases with pressure. This trend is consistent with studies in the literature done at subatmospheric or atmospheric pressure [13] [11] [20] [27]. For given conditions (constant P_{sat}), these said trends are easily analyzed with (Eq. 18) which allows to determine the experimental heat transfer coefficients. Thus, the proposed correlations correctly capture the relationships between HTC (h), working pressure (P_{sat}) and heat flux ($\dot{q}$) verified extensively in the literature, for different pressure and/or temperature conditions.

The constants and coefficients of the correlations (Eq. 28) and (Eq. 29) are specific to the evaporator studied (Fig.2) and to the domain covered by the experimental program described in subsection 2.3. In order to extend their areas of validity, they are evaluated by fitting their constants and coefficients with different experimental data obtained at low pressure by other authors (Table 9).

Table 9 : Constants and coefficients fitted to experimental data from the literature

	Constants and coefficients fitted						
Data base	**C**	$\mathbf{a_1}$	$\mathbf{a_2}$	$\mathbf{a_3}$	$\mathbf{a_4}$	$\mathbf{a_5}$	**Areas**
Zajaczkowski et al. [11]	$1.839 \cdot 10^{-3}$	0,111	-0.798	-0.405	-1.543	0.988	Pooling boiling region
Chang et al. [13]	$2.299 \cdot 10^{-3}$	0.111	-0.798	-0.405	-1.543	0.988	Pooling boiling region
Chang et al. [13]	$4.818 \cdot 10^{-6}$	-0.385	-0.871	0.756	-2.002	1.406	Intermittent region

621

622 The experimental data from Zajaczkowski et al. [11] and Chang et al. [13] are compared
623 with the corresponding values estimated by the new correlations (Table 9), as shown in Fig.9.

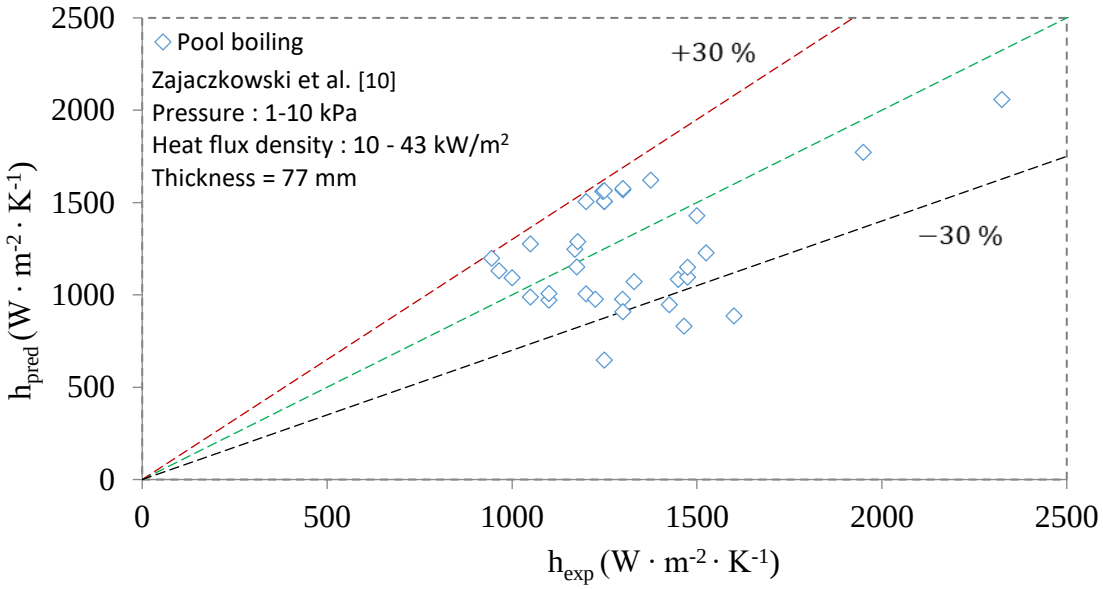

(a)

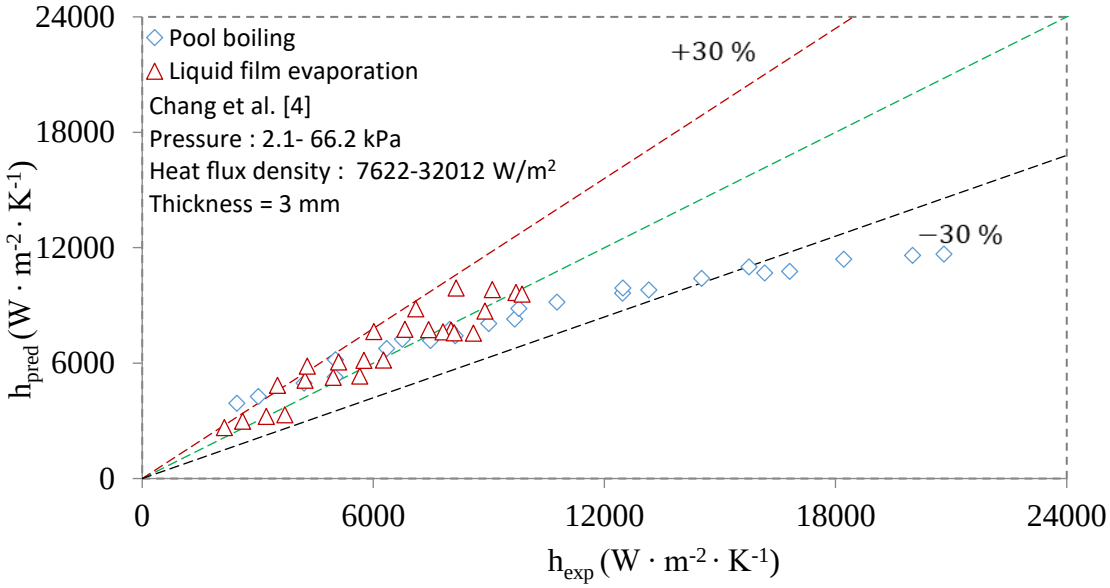

(b)

Figure 9 : Comparison between experimental HTC (h_{exp}) from the literature and HTC calculated (h_{pred}) by the new correlations

According to Fig.9, the developed pool boiling correlation predicts 71% (with MRE =-1%, MAE=5%) and 85% (with MRE = -2%, MAE = 4%) of the respective Zajaczkowski et al. [11] and Chang et al. [13] experimental databases. As for the liquid film evaporation correlation, it predicts 92% (with MRE =2%, MAE = 2%) of the experimental data from Chang et al. [13] (Intermittent region). Thus, from these results, it can be inferred that the dimensionless numbers found in this work are relevant for correlating the pool boiling and liquid film evaporation HTC at low pressure.

It is believed that the proposed correlations could then be used more widely. By keeping the dimensionless numbers and fitting them with more data one would be able to predict all the HTC of water at subatmospheric pressure and at higher pressure since these numbers consider many relevant parameters. As a result, these new correlations and/or the dimensionless numbers used should allow the design of various two-phase evaporators.

7. Conclusion

Raw experimental data, obtained in order to study heat transfer phenomena during the vaporization of water at pressures ranging from 0.7 to 1.7 kPa in a vertical evaporator channel with smooth plates of standard size (0.2 m wide x 0.5 m high) included inside a thermosyphon loop mimicking a sorption system are processed and exploited.

A graphical and statistical comparison between the HTC from the experimental database and the HTC estimated by empirical correlations from the literature is made. Among the correlations used, only those of Dittus-Boelter (Eq.1), Kruzylin (Eq. 3) and Chang (Eq. 6 and Eq. 7) gave good statistical results but still, show poor performance (Table 10).

Table 10: Results obtained from the statistical comparison between the experimental HTC and the HTC predicted by Dittus-Boelter (Eq.1), Kruzylin (Eq. 3) and Chang (Eq. 6 and Eq. 7) correlations.

	Pool boiling zone			
Correlations	MAE [%]	MRE [%]	τ_{30}[%]	r [−]
Dittus-Boelter [19]	24	7	73	0.67
Kruzylin [11]	28	− 26	54	0.64
Chang [13]	29	8	69	0.57
	Liquid film evaporation zone			
Correlations	MAE [%]	MRE [%]	τ_{30}[%]	r
Dittus-Boelter [19]	27	12	68	0.72
Chang [13]	40	13	54	0.50

Based on a rigorous dimensional analysis, two news methodical correlations to predict the pool boiling and liquid film evaporation HTC are developed by fitting the experimental database by mean of the least squares method. Unlike the empirical correlations in the literature, these new models consider among others the thermophysical properties of the fluid (saturation pressure, hydrostatic pressure), the heat flow, the parietal superheating, the filling height of the channel and the geometrical parameters (boundary conditions). They therefore involve various

dimensionless numbers of great importance for the dimensioning of two-phase heat exchangers and the optimization of their design like for example, the form factor (e/H_l), which it is believed to help finding the correct filling ratio and channel thickness to obtain the best system performance. Moreover, it is believed that the proposed correlations could then be used more widely by keeping the dimensionless numbers and fitting them with more data. Currently, the new correlations predict 86% (with MAE = 19%, MRE = 3%, $r = 0.79$) and 83% (with MAE = 18%, MRE = 2%, $r = 0.84$) of the experimental data in τ_{30} respectively.

To extend their validity domains, the new correlations are evaluated by fitting the constants and coefficients with experimental data from Zajaczkowski et al. [11] and Chang et al. [13] (Table **9**). The pool boiling correlation correctly predicts 71% (with MRE = -1%, MAE = 5%) and 85% (with MRE = -2%, MAE = 4%) of the databases of respective authors. As for the liquid film evaporation correlation, it predicts 92% (with MRE = 2%, MAE = 2%) of the experimental data from [13] (Intermittent region). Thus, from these satisfactory results, the new proposed models constitute a first step towards the development of tools to assist in the sizing of two-phase heat exchangers and the optimization of their operation.

In order to allow a generalization and to better understand the impact of all the parameters taken into account, experimental test campaigns with a wider range of pressures are envisaged in order to make the correlations more robust and to allow the insertion of dimensionless numbers removed from (Eq. 26) due to their small variation. Research on the decisive effect that non-condensable gases such as air can have on heat transfer by vaporization at sub-atmospheric pressure also seems necessary. Tests will be also performed with other fluids.

Acknowledgements :

The authors wish to thank the “Ministère des Affaires Etrangères de la France” (French Ministry of Foreign Affairs) for funding research stays in Lafset through a cooperation grant with Senegal (Service de Coopération et d'Action Culturelle (SCAC) of the French Embassy in Dakar). This project focuses on compact plate evaporators using water as refrigerant in order to properly size and design them.

Appendix A: Dimensional Analysis Approach

The main step of the dimensional analysis is the choice of fundamental quantities, i.e., the quantities according to which the dimensions of the independent physical parameters governing the studied phenomena are expressed. In the international system, the fundamental quantities are the mass M, the length L and the time T. In heat transfer problems, as in the case of this study, it is necessary to add a fourth dimension Θ. To go back to the dimensionless numbers that characterize the physical problem under study, this requires the free choice of the repeated variables, provided that they are dimensionally independent and that their dimensions cover all the fundamental dimensions (the determinant of the matrix is non-zero) [18]. The repeated variables $(e, \mu_l, \rho_l, c_{p_l})$ and the non-repeated variables $(H_l, \mu_v, \rho_v, \rho_b, \Delta h_{lv}, \sigma, g, \lambda_l)$ form the matrix with dimensions D (Table A.1). The repeated variables form the central matrix C (blue background) and the unrepeated variables form the residual matrix R (grey background).

Table A.1 : Matrix with dimensions D.

	h	H_l	μ_v	ρ_v	ρ_b	G_v	σ	g	λ_l	e	μ_l	ρ_l	c_{p_l}
M	1	0	1	1	1	1	1	0	1	0	1	1	0
L	0	1	-1	-3	-3	- 2	0	1	1	1	-1	-3	2
T	-3	0	-1	0	0	- 1	-2	-2	-3	0	-1	0	-2

Θ	-1	0	0	0	0	0	0	0	-1	0	0	0	1

In order to find the dimensionless groupings, linear combinations between the rows of the matrix with dimensions D (Table A.1) to transform the central matrix C into an identity matrix are made. These operations lead to the matrix with modified dimensions Dm (Table A.2) an identity matrix (modified central matrix Cm), the dimensionless numbers characterizing the physical phenomenon can be written, based on the coefficients contained in the columns of the new residual matrix R (modified residual matrix Rm). Each non-repeated variable represented by G_i (i.e. each column of the modified residual matrix) forms a dimensionless number π_i (Eq. A.1) [18].

Table A.2 : Matrix with modified dimensions Dm

h	H_l	μ_v	ρ_v	ρ_b	G_v	σ	g	λ_l	e	μ_l	ρ_l	c_{p_l}
-1	1	0	0	0	-1	-1	-3	0	1	0	0	0
1	0	1	0	0	1	2	2	1	0	1	0	0
0	0	0	1	1	0	-1	-2	0	0	0	1	0
1	0	0	0	0	0	0	0	1	0	0	0	1

$$\pi_i = \frac{G_i}{e^{a_{i1}}\ \mu_l^{a_{i2}}\ \rho_l^{a_{i3}}\ c_{pl}^{a_{i4}}} \tag{A.1}$$

The process relationship (Eq.24) can now be expressed in dimensionless form by the Eq. (A.2).

$$\pi_h = \frac{h\ e}{\mu_l\ \ c_p} = F\left(\begin{array}{c} \pi_{H_l} = \frac{H_l}{e};\ \pi_{\mu_v} = \frac{\mu_v}{\mu_l};\ \pi_{\rho_v} = \frac{\rho_v}{\rho_l};\ \pi_{\rho_b} = \frac{\rho_b}{\rho_l}; \\ \pi_{G_v} = \frac{G_v\ e}{\mu_l};\ \pi_\sigma = \frac{\sigma\ e\ \rho_l}{\mu_l^2}; \\ \pi_g = \frac{\rho_l^2 g\ e^3}{\mu_l^2};\ \pi_{\lambda_l} = \frac{\lambda_l}{\mu_l\ c_{p_l}} \end{array}\right) \tag{A.2}$$

The space of the dimensionless groupings (π_i) obtained Eq. (A.2) is modified in order to simplify the interpretation of the dimensionless numbers and to try to understand the physical phenomena involved in the process of boiling and evaporation at subatmospheric pressure in a PHE. These rearrangements, which consist of raising some to different powers, multiplying or dividing them, adding or subtracting them, make it possible to go from Eq. (A.2) to (Eq.25).

References

[1] K. Amir A. and M. Norbert , "Comparing water (R718) to other refrigerants".*ASME International Mechanical Engineering Congress and Exposition, December 14, 2007, https://doi.org/10.1115/IMECE2006-13341.*

[2] J. Seiler, R. Volmer, D. Krakau, J. Pöhls, F. Ossenkopp, L. Schnabel and A. Bardow, "Capillary-assisted evaporation of water from finned tubes – Impacts of experimental setups and dynamics," *Applied Thermal Engineering 165 (2020) 114620. https://doi.org/10.1016/j.applthermaleng.2019.114620.*

[3] K. Amir A. and M. Norbert , "Comparing water (R718) to other refrigerants".*ASME International Mechanical Engineering Congress and Exposition, December 14, 2007, https://doi.org/10.1115/IMECE2006-13341.*

[4] F. Giraud, "Vaporization of water at subatmospheric pressure:fundamentals of boiling phenomena and path towards the design of compact evaporators for sorption chillers," Thermique et Energétique, Ph.D. Thesis, L'institut National des Sciences Appliquées de Lyon, Lyon, France, 2015.

[5] F. Giraud, C. Toublanc, R. Rullière, J. Bonjour and . M. Clausse, "Experimental study of water vaporization occurring inside a channel of a smooth plate-type heat exchanger at subatmospheric pressure," *Applied Thermal Engineering 106 (2016) 180-191. http://dx.doi.org/10.1016/j.applthermaleng.2016.05.151.*

[6] S. Michaie, R. Rullière and J. Bonjour, "Towards a more generalized understanding of pool boiling at low pressure : Bubble dynamics for two fluids in states of thermodynamic similarity," *Experimental Thermal and Fluid Science 101 (2019) 217-230. https://doi.org/10.1016/j.expthermflusci.2018.10.009.*

[7] D. Triché, "Étude numérique et expérimentale des transferts couplés de masse et de chaleur dans l'absorbeur d'une machine à absorption ammoniac-eau," Thèse, Mécanique des fluides, Énergétique, Procédés,Université Grenoble Alpes, 2016, 199.

[8] F. A. Mota, E. P. Carvalho and M. A. Ravagnani, "Chapter 7 : Modeling and Design of Plate Heat Exchanger," in *Heat Transfer Studies and Applications 165 (2012) 199, Janeza Trdine 9, 51000 Rijeka, Croatia, InTech.*

[9] F. Tàboas, M. Vallès, M. Bourouis and A. Coronas, "Assessment of boiling heat transfer and pressure drop correlations of ammonia/water mixture in a plate heat exchanger," *International journal of refrigeration 35 (2012) 633-644. doi:10.1016/j.ijrefrig.2011.10.003.*

[10] Z. H. Ayub, T. S. Khan, S. Salam, K. Nawaz, A. H. Ayub and M. S. Khan, "Literature survey and a universal evaporation correlation for plate type heat exchangers," *International Journal of Refrigeration 99 (2019) 408-418. https://doi.org/10.1016/j.ijrefrig.2018.09.008.*

[11] B. Zajaczkowski, T. Halon and Z. Krolicki, "Experimental verification of heat transfer coefficient for nucleate boiling at sub-atmospheric pressure and small heat fluxes," *Heat Mass Transfer, 52 (2016) 205–215. https://doi.org/10.1007/s00231-015-1549-8.*

[12] F. Giraud, R. Rullière, C. Toublanc, M. Clausse and J. Bonjour, "Experimental evidence of a new regime for boiling of water at subatmospheric pressure," *Experimental*

Thermal and Fluid Science 60 (2015) 45-53. http://dx.doi.org/10.1016/j.expthermflusci.2014.07.011.

[13] S. W. Chang, D. C. Lo, K. F. Chiang and C. Y. Lin, "Sub-atmospheric boiling heat transfer and thermal performance of two-phase loop thermosyphon," *Experimental Thermal and Fluid Science 39 (2012) 134-147. doi:10.1016/j.expthermflusci.2012.01.017.*

[14] L. Schnabel, C. Scherr and C. Weber, "Water as refrigerant – Experimental evaluation of boiling characteristics at low temperatures and pressures".*VII Minsk International Seminar "Heat Pipes, Heat Pumps, Refrigerators, Power Sources", Minsk, Belarus, September 8-11, 2008.*

[15] F. Giraud, R. Rullière, C. Toublanc, M. Clausse and J. Bonjour, "Subatmospheric pressure boiling on a single nucleation site in narrow vertical spaces," *International Journal of Heat and Fluid Flow 58 (2016) 1-10. http://dx.doi.org/10.1016/j.ijheatfluidflow.2015.12.002.*

[16] F. Giraud and B. Tréméac, "Influences of confinement on subatmospheric water vaporization phenomena in a vertical rectangular channel," International Journal of Heat and Mass Transfer 145 (2019) 118725.

[17] F. Giraud, P. Vallon and B. Tremeac, "Experimental study of water vaporization occurring inside the channel of a smooth-plate type heat exchanger connected to an adsorber and comparison with trends observed in absorption configuration".*International Journal of of refrigeration 77 (2017) 60-74, http://dx.doi.org/10.1016/j.ijrefrig.2017.02.021.*

[18] G. Delaplace, K. Loubière, F. Ducept and R. Jeantet, Modélisation en génie des procédés par analyse dimensionnelle. Méthode et exemples résolus, Paris: Editions Lavoisier TEC et DOC, 2014.

[19] S. Bengt, "Chapter Two - Advanced heat transfer topics in complex duct flows, Advances in Heat Transfer,49 (2017) 37-89, https://doi.org/10.1016/bs.aiht.2017.09.001".

[20] L.-H. Yu , S.-X. Xu , G.-Y. Ma and J. Wang, "Experimental research on water boiling heat transfer on horizontal copper rod surface at sub-Atmospheric pressure," *Energies 8 (2015) 10141-10152; doi:10.3390/en80910141.*

[21] T. Baki , "Boiling pure fluids at sub atmospheric pressures," *International Journal of Mathematics and Computers in Simulation, 14 (2020) 87-91, DOI: 10.46300/9102.2020.14.12.*

[22] S. A. Alavi Fazel and S. Roumana, "Pool boiling heat transfer to pure liquids," *Continuum Mechanics, Fluids, Heat, n° ISBN : 978-960-474-158-8 (2010) 211-216.*

[23] K. Zhang, Y. Hou, W. Tian, Y. Fan, G. Su and S. Qiu, "Experimental investigations on single-phase convection and steam-water two-phase flow boiling in a vertical rod

bundle, Experimental Thermal and Fluid Science, 80 (2017) 147–154. https://doi.org/10.1016/j.expthermflusci.2016.08.018".

[24] F. Giraud, R. Rullière, C. Toublanc, M. Clausse and J. Bonjour, "Experimental evidence of a new regime for boiling of water at subatmospheric pressure," *Experimental Thermal and Fluid Science 60 (2015) 45-53. http://dx.doi.org/10.1016/j.expthermflusci.2014.07.011.*

[25] J. Bonjour, F. Boulanger, D. Gentile and M. Lallemand, "Etude phénoménologique de l'ébullition en espace confiné à partir d'un site de nucléation isolé," *Rev. Gén. Therm. 36 (1997) 562-572.*.

[26] R. L. Amalfi, F. Vakili-Farahani and J. R. Thome , "Flow boiling and frictional pressure gradients in plate heat exchangers: part 2, comparison of literature methods to database and new prediction methods," *International Journal of Refrigeration 61 (2016) 185-203. http://dx.doi.org/10.1016/j.ijrefrig.2015.07.009.*

[27] I. S. Kiyomura, T. S. Mogaji, L. L. Manetti and M. E. Cardoso, "A predictive model for confined and unconfined nucleate boiling heat transfer coefficient," *Applied Thermal Engineering 127 (2017) 1274–1284; http://dx.doi.org/10.1016/j.applthermaleng.2017.08.135.*

715

716